IEEE Access
Multidisciplinary | Rapid Review | Open Access Journal

Received December 8, 2021, accepted December 26, 2021, date of publication December 28, 2021,
date of current version January 19, 2022.

*Digital Object Identifier 10.1109/ACCESS.2021.3139089*

# Kinematic and Stiffness Modeling of a Novel 3-DOF *RPU+UPU+SPU* Parallel Manipulator

**NIJIA YE AND BO HU**
School of Mechanical Engineering, Yanshan University, Qinhuangdao 066004, China
Parallel Robot and Mechatronic System Laboratory of Hebei Province, Yanshan University, Qinhuangdao 066004, China

Corresponding author: Bo Hu (hubo@ysu.edu.cn)

This work was supported in part by the Hebei Provincial Natural Science Foundation under Grant E2020203027 and Grant E2021203019, in part by the Central Government Guiding Local Science and Technology Development Fund Project of Hebei Province under Grant 206Z7602G, and in part by the Youth Foundation of Science and Technology of Higher Education of Hebei Province under Grant QN2020230.

**ABSTRACT** A novel 3-degrees of freedom (DOF) *RPU+UPU+SPU* parallel manipulator (PM) is proposed in this study, and its complete kinematics and stiffness are studied systematically. First, the architecture description is discussed, and the inverse and the forward positional posture analysis are studied based on the constraints in the PM. Second, the Jacobian matrix, the velocity model, the Hessian matrix and the acceleration model are derived in explicit and compact forms. Third, based on the virtual work principle, the static model and the deformation decompose method, the stiffness model is built. Meanwhile, the stiffness matrix and the compliance matrix are obtained. Finally, the correctness of the models built in this study are verified by simulative PMs. This study is expected to provide new ideas for the design of PM machine tools.

**INDEX TERMS** 3-DOF parallel manipulator, complete kinematic analysis, stiffness modeling.

## I. INTRODUCTION

As an essential branch of limited-DOF PMs, 3-DOF PMs have attracted much attention due to their excellent merits, such as simplicity in structure, low cost of manufacturing and easy control [1]. According to these characteristics, 3-DOF PMs are widely used in the field of machine tool. In this field, one of the famous inventions is a *3PRS PM* [2], which is the primary mechanism of Sprint Z3. In addition, Neumann proposed a *3UPS+UP PM* (Tricept) [3], which owns high dynamics, stiffness and ample workspace. Then, the inventor presented the concept of a *2UPR+SPR PM* (Exechon) [4], which can be applied to fill in the gap between the traditional machine tools and the industrial robots.

In recent years, the design and analysis of 3-DOF PMs are still a hot topic in academia. By integrating one active *UPU* leg into a passive one, Huang *et al.* [5] designed a modified Tricept robot-TriVariant. Li *et al.* [6] presented an A3 head applied to manufacturing large structural components. Wang *et al.* [7] proposed a 3*PUU* PM possessing good motion/force transmissibility and orientation capability, and studied its optimal design [8]. Sun synthesized some 3-DOF PMs [9], and presented a simple and highly visual approach for type synthesis of 3-DOF over-constraint PMs [10]. Lu *et al.* [11] innovated some 3-DOF PMs with planar sub-chains using the revised digital topological graphs and arrays. Gallardo and Rodriguez [12] proposed a 3-DOF 3*RPRRC+RRPRU* robot. Jing *et al.* [13] designed a redundant collaborative manipulator containing a class of 3-DOF PM heads with high rotational capability. Hu *et al.* [14] studied the kinematic characteristics of a 3-DOF 3*UPU+UP* PM with coupling parallel platforms. Yang *et al.* [15] discussed the kinematics of a 3-DOF 3*PPS* PM. Here and throughout, *R*, *P*, *U* and *S* denotes a revolute joint, a prismatic joint, a universal joint and a sphere joint, respectively.

However, existing 3-DOF PMs are not enough to satisfy the continuous innovation demands of the machine tools. Especially in recent years, the demands for irregular shape components in the aerospace field are increased, the stiffness requirements of each direction are inconsistent during processing. Therefore, the demands for innovative design of asymmetric 3-DOF PMs are increased significantly. In addition, existing asymmetric 3-DOF PMs virtually all contain over-constraint wrenches, which have high requirements for manufacture and assembly. Once the manufacture and assembly are slightly careless, it will seriously affect the accuracy of the machine tools. Compared with over-constraint PMs, non-over-constraint PMs have a simple structure and lower

The associate editor coordinating the review of this manuscript and approving it for publication was Guilin Yang.

requirements in manufacture and assembly, which can better adapt to different working requirements and realize specific requirements. However, so far there are few reports for asymmetric non-over-constraint 3-DOF PMs, which provide motivations for this study.

Stiffness refer to the ability to resist elastic deformations, which is one of the PM's most important performance parameters and a core factor that must be considered in the machine tool design. Many scientists commit to studying the stiffness of PM. Gosselin [16] established the stiffness model of PMs considering the active factors. Huang *et al.* [17] studied the stiffness of a tripod-based PM containing the rigidity of the machine frame. Liu *et al.* [18] conducted an optimum design of a 3-DOF spherical PM concerning the conditioning and stiffness indices. Zhang and Gosselin [19] and Zhang [20] built the kinetostatic and stiffness model for some 3, 4 and 5-DOF PMs. Han *et al.* [21] analyzed the stiffness of a 4-DOF PM basing on the screw theory. Merlet [22], a famous French mechanism scholar, pointed out that: for lack of considering the role of constraints, many mechanism analysis problems may exist faultiness. For example, constrained forces/torques are bound to cause deformations of the leg and then significantly affect the stiffness of PMs. Therefore, they must be considered when stiffness modeling. Unfortunately, the previously mentioned researches have ignored.

In recent years, the influences of constraints on the force and stiffness of limited-DOF PMs is gratifying caused extensive concerns. Wojtyra [23] used the singular value decomposition and QR decomposition methods to solve the joint constraint reaction forces of over-constraint PMs. Utilizing the instantaneous screw theory, Lian *et al.* [24] formulated the stiffness model of a 5-DOF PM considering the gravitational effects. Sun *et al.* [25] established the semi-analytic stiffness model of a hybrid manipulator as a friction stir welding robot composed of a 3-DOF PM module and a 2-DOF rotating head. Hu and Huang [26] proposed the constraints and deformations decomposition matching method for solving the force and stiffness problems of limited-DOF PMs. Liu *et al.* [27] established the static and stiffness models of over-constraint PMs by combining the weighted Moore-Penrose inverse. Li *et al.* [28] studied the analytic solution of the elastic stiffness model for limited-DOF PMs using the geometric algebra and strain energy methods. Cao and Ding [29] solved the joint reaction forces of an over-constraint PM with flexible joints. Considering both constrained wrenches and active wrenches, Li and Xu [30] presented the stiffness characteristics of a 3-DOF 3-*PUU* translational PM; Chen *et al.* [31] systematically studied the stiffness of a 6-DOF 3*CPS* PM; Shan and Hen [32] investigated the stiffness of a 2(3*PUS*+*S*) PM with two moving platforms. Each of the above method has its own merits, which lays solid foundations for this study.

For these reasons, this study proposes a novel asymmetric non-over-constraint 3-DOF *RPU+UPU+SPU* PM, the complete kinematics and stiffness analysis of this novel PM are carried out, and is expected to provide new ideas for the design of PM machine tools. Since this novel PM has three different types of legs, and each leg contains different constraints, the researches of the complete kinematic analysis and stiffness analysis are still challenging works.

The remainder of this study is organized as below. In section II, the architecture description of the proposed PM is given, then the constraints analysis is performed. In section III, the complete positional posture analysis is discussed, then the velocity and acceleration kinematics analysis are studied. In section IV, the stiffness model is established. In section V, numerical examples are given to verify the correctness of the analytic models established in this study. Finally, conclusions are drawn.

## II. DESCRIPTION OF THE RPU+UPU+SPU PM

### A. MECHANISM ARCHITECTURE

The proposed PM includes a moving platform $m$, a base platform $B$ and three legs $r_i(i = 1, 2, 3)$, as shown in FIGURE 1. The architectures of $m$ and $B$ are equilateral triangles. Each $r_i(i = 1, 2, 3)$ has one active $P$ joint. Each $U$ joint is composed of two perpendicularly intersecting $R$ joints.

In $r_1$, the bottom of the $P$ joint is attached to $B$ by a $R$ joint whose axis is in the plane of $B$ and perpendicular to one side of $B$. The other end of the $P$ joint is fixed to $m$ with a $U$ joint. In this $U$ joint, one $R$ joint is parallel with the $R$ joint in the plane of $B$, the remaining one $R$ joint is perpendicular to $m$.

In $r_2$, the bottom of the $P$ joint is attached to $B$ by a $U$ joint. In this $U$ joint, one $R$ joint is perpendicular to $B$, the remaining one $R$ joint is vertical to $r_2$. The other end of the $P$ joint is fixed to $m$ with a $U$ joint. In this $U$ joint, one $R$ joint is parallel with the $R$ joint that is perpendicular to $r_2$, the remaining one $R$ joint is in the plane of $m$ and perpendicular to one side of $m$.

In $r_3$, the bottom of the $P$ joint is attached to $B$ by a $S$ joint. The other end of the $P$ joint is fixed to $m$ with a $U$ joint.

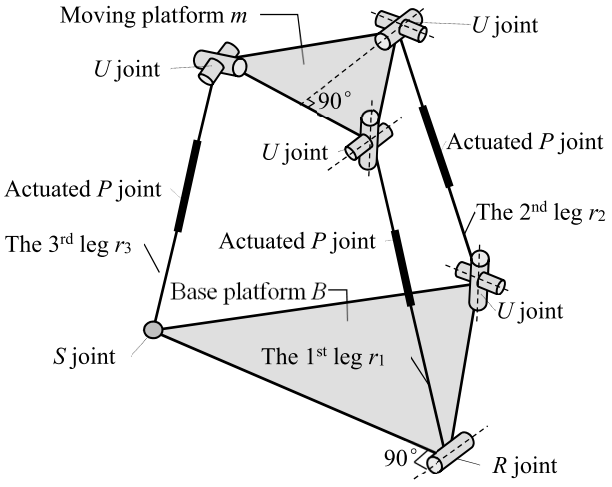


**FIGURE 1.** A novel RPU+UPU+SPU PM.

The mechanism under study is a 3-DOF PM, as can be calculated by the revised Kutzbach-Grübler equation [1]:

$$M = 6(n - g - 1) + \sum_{i=1}^{g} m_i - m_0 \tag{1}$$

where $M$ is the DOF number of the PM, $n$ is the number of links in the PM, $g$ is the number of joints, $m_i$ is the DOF number of the $i$-th joint and $m_0$ is the passive DOF. For the proposed PM, there are one $S$ joint, four $U$ joints, one $R$ joint and three $P$ joints, $n = 8$ and $g = 9$. Application of (1), it leads to:

$$M = 6 \times (8 - 9 - 1) + (3 \times 1 + 2 \times 4 + 1 \times 4) - 0 = 3 \tag{2}$$

### B. FRAMES OF REFERENCE, CONSTRAINT JUDGMENT AND VECTOR REPRESENTATION

To simplify expression, $B_1$, $B_2$ and $B_3$ are named as the vertices of $B$. Denote $O$-$XYZ$ be the inertial frame. $O$ is the center of $B$. $X$ is parallel with $B_1B_3$. $Y$ also lies in the plane of $B$ while $Z$ is normal to $B$ and points upward, thereby forming a right-handed orthogonal frame. $A_1$, $A_2$ and $A_3$ are named as the vertices of $m$. Denote $O'$ -$X'$ $Y'$ $Z$ be the moving frame. $O'$ is the center of $m$. $X'$ is parallel with $A_1A_3$. $Y'$ also lies in the plane of $m$ while $Z'$ is normal to $m$ and points upward, thereby forming a right-handed orthogonal frame. As shown in FIGURE 2.

Let $R_{ij}$ be the $j$-th $R$ joint from $B$ to $m$ in $r_i (i = 1, 2)$. Based on the mechanism architecture, following relationships can be written:

$$\begin{aligned} &R_{11} \parallel Y, R_{11} \perp r_1, R_{12} \parallel R_{11}, R_{13} \perp R_{12}, R_{13} \parallel Z' \\ &R_{21} \parallel Z, R_{22} \perp R_{21}, R_{22} \perp r_2, R_{23} \parallel R_{22}, R_{24} \perp R_{23}, R_{24} \parallel Y' \end{aligned} \tag{3}$$

where $\parallel$ and $\perp$ denotes parallel and perpendicular constraints, respectively.

Because of the above relationships, there are constrained wrenches in the proposed PM, which can be determined by the geometrical rules [33], [34]:

(a) In each leg, the constrained forces should be perpendicular to all $P$ joints and coplanar with all $R$ joints.

(b) In each leg, the constrained torques should be perpendicular to all $R$ joints.

Utilizing the rules (a) and (b), the constrained forces/ torques in this PM can be determined. In $r_1$, there exists one constrained force $\boldsymbol{F_{p1}}$ which is parallel with $R_{12}$ and $R_{11}$,and one constrained torque $\boldsymbol{T}_1$ which is perpendicular to $R_{12}$ and $R_{13}$ as well as passes through $A_1$. In $r_2$, there exists one constrained force $\boldsymbol{F_{p2}}$ which is parallel with $R_{23}$ and $R_{22}$ as well as passes through a point $C$. Where $C$ is an intersection point of $R_{21}$ and $R_{24}$. As shown in FIGURE 2.

To simplify expression, denote $\boldsymbol{\delta_i}$ be the unit vector of $r_i$, $\boldsymbol{e_i}$ be the vector from $O'$ to $A_i$, $F_{pi}/T_1$ be the value of $\boldsymbol{F}_{pi}/\ \boldsymbol{T}_1$, $\boldsymbol{f_i}/\ \boldsymbol{\tau}_1$ be the unit vector of $\boldsymbol{F_{pi}}/\boldsymbol{T}_1$, $\boldsymbol{d_i}$ be the vector from $O'$ to an arbitrary point on $\boldsymbol{F}_{pi}$. As shown in FIGURE 2.

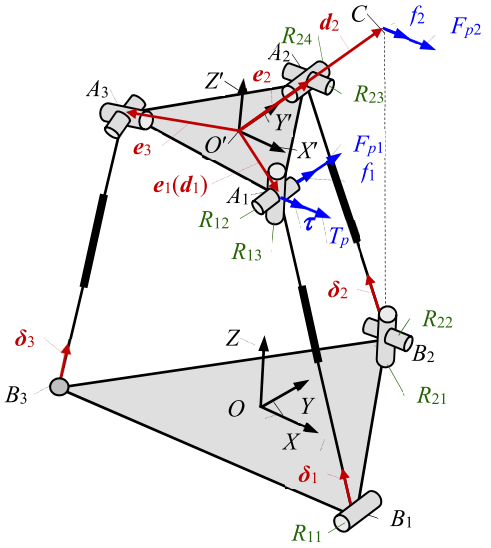


**FIGURE 2.** Frames of reference and vector representation.

## III. KINEMATIC ANALYSIS OF THE RPU+UPU+SPU PM

### A. COMPLETE POSITIONAL POSTURE MODEL

In limited-DOF PMs, there exists coupling relationships between the 6-dimensional positional posture of the moving platform, which need to be analyzed first before the kinematic modeling. Denote $\boldsymbol{R_{ij}}$, $\boldsymbol{X}$, $\boldsymbol{Y}$, $\boldsymbol{Z}$, $\boldsymbol{X'}$, $\boldsymbol{Y'}$ and $\boldsymbol{Z'}$ be the unit vector of $R_{ij}$, $X$, $Y$, $Z$, $X'$, $Y'$ and $Z'$ in$\{O$-$XYZ\}$, respectively. Based on (3), it leads to:

$$\begin{aligned} &\boldsymbol{R}_{11} = \boldsymbol{Y} = \begin{bmatrix} 0 & 1 & 0 \end{bmatrix}^{\mathrm{T}}, \quad \boldsymbol{R}_{11} \cdot \boldsymbol{B}_1\boldsymbol{A}_1 = 0, \\ &\boldsymbol{R}_{12} = \boldsymbol{R}_{11}, \quad \boldsymbol{R}_{13} \cdot \boldsymbol{R}_{12} = 0 \\ &\boldsymbol{R}_{13} = \boldsymbol{Z'}\dot{\boldsymbol{R}}_{21} = \boldsymbol{Z} = \begin{bmatrix} 0 & 0 & 1 \end{bmatrix}^{\mathrm{T}}, \quad \boldsymbol{R}_{22} \cdot \boldsymbol{R}_{21} = 0, \\ &\qquad \boldsymbol{R}_{22} \cdot \boldsymbol{B}_2\boldsymbol{A}_2 = 0 \\ &\boldsymbol{R}_{23} = \boldsymbol{R}_{22}, \quad \boldsymbol{R}_{24} \cdot \boldsymbol{R}_{23} = 0, \quad \boldsymbol{R}_{24} = \boldsymbol{Y'} \end{aligned} \tag{4}$$

Let $\boldsymbol{A_i}$ and $\boldsymbol{B_i}$ $(i = 1, 2, 3)$ be the vector of $A_i$ and $B_i$ in$\{O$-$XYZ\}$. And denote ${}^m\boldsymbol{A}_i$ $(i = 1, 2, 3)$ be the vector of $A_i$ in $\{O'\ X'\ Y'\ Z'\ \}$. Based on the mechanism architecture, $\boldsymbol{B_i}$ and ${}^m\boldsymbol{A}_i$ can be expressed as below:

$$\begin{aligned} &\boldsymbol{B}_1 = \frac{1}{2}\begin{bmatrix} \sqrt{3}E \\ -E \\ 0 \end{bmatrix}, \quad \boldsymbol{B}_2 = \begin{bmatrix} 0 \\ E \\ 0 \end{bmatrix}, \quad \boldsymbol{B}_3 = -\frac{1}{2}\begin{bmatrix} \sqrt{3}E \\ E \\ 0 \end{bmatrix} \\ &{}^m\boldsymbol{A}_1 = \frac{1}{2}\begin{bmatrix} \sqrt{3}\,e \\ -e \\ 0 \end{bmatrix}, \quad {}^m\boldsymbol{A}_2 = \begin{bmatrix} 0 \\ e \\ 0 \end{bmatrix}, \quad {}^m\boldsymbol{A}_3 = -\frac{1}{2}\begin{bmatrix} \sqrt{3}\,e \\ e \\ 0 \end{bmatrix} \end{aligned} \tag{5}$$

where $E$ is the distance from $O$ to $B_i$ and $e$ is the distance from $O'$ to $A_i$. Let ${}^m_B\boldsymbol{R}$ be the rotational transformation matrix from $\{O$-$XYZ\}$ to $\{O'$ -$X'$ $Y'$ $Z'\}$ and $\boldsymbol{O'}$ be the vectors of $O'$ in$\{O$-$XYZ\}$. Then, $\boldsymbol{A_i}$ $(i = 1, 2, 3)$ can be expressed as below:

$$\boldsymbol{A}_i = {}^m_B\boldsymbol{R}\,{}^m\boldsymbol{A}_i + \boldsymbol{O'}, \quad {}^m_B\boldsymbol{R} = \begin{bmatrix} x_l & y_l & z_l \\ x_m & y_m & z_m \\ x_n & y_n & z_n \end{bmatrix},$$

$$\boldsymbol{O}' = \begin{bmatrix} X_o \\ Y_o \\ Z_o \end{bmatrix} \tag{6}$$

From (4), (5) and (6), the positional posture coupling relationships of $m$ for the proposed PM can be obtained.

$$\begin{aligned} z_m &= 0 \\ Y_o &= \frac{1}{2}\left(-E - \sqrt{3}\, ex_m + ey_m\right) \\ X_o &= \frac{y_l}{y_m}\left(Y_o - E\right) \end{aligned} \tag{7}$$

Furthermore, set ${}^{m}_{B}\boldsymbol{R}$ be formed by $YXZ$-type Euler rotations with $\alpha$, $\beta$ and $\lambda$ as three Euler angles. Combined with (7), ${}^{m}_{B}\boldsymbol{R}$ can be specific expressed as below:

$${}^{m}_{B}\boldsymbol{R} = \begin{bmatrix} c_\alpha c_\lambda & -c_\alpha s_\lambda & s_\alpha \\ s_\lambda & c_\lambda & 0 \\ -s_\alpha c_\lambda & s_\alpha s_\lambda & c_\alpha \end{bmatrix} \tag{8}$$

where $s_\theta$ denotes sin $(\theta)$ and $c_\theta$ denotes cos $(\theta)$ with $\theta$ is $\alpha$ or $\lambda$, then (7) can be simplified as below:

$$\begin{aligned} \beta &= 0 \\ Y_o &= \frac{1}{2}\left(-E - \sqrt{3}\, es_\lambda + ec_\lambda\right) \\ X_o &= \frac{-c_\alpha s_\lambda}{2c_\lambda}\left(3E + \sqrt{3}\, es_\lambda - ec_\lambda\right) \end{aligned} \tag{9}$$

Equation (9) shows the explicit coupling relationships between the 6-dimensional positional posture of $m$. According to (9), $\alpha$, $\lambda$ and $Z_o$ can be considered as the independent kinematic parameters for this PM.

Complete positional posture analysis includes the forward and inverse analysis. When the actuators are set, the positional posture of the moving platform can be determined by the forward model. By contrast, the inverse analysis determines the required actuators variables from a given positional posture of the moving platform.

For the proposed PM, $r_i$ $(i = 1, 2, 3)$ can be derived by the following formulas:

$$\begin{aligned} r_i &= |\boldsymbol{A}_i - \boldsymbol{B}_i| \\ r_1^2 &= X_o^2 + Y_o^2 + Z_o^2 + E^2 + e^2 - \sqrt{3}EX_o + EY_o \\ &\quad + \sqrt{3}\, e(x_l X_o + x_m Y_o + x_n Z_o) - e(y_l X_o + y_m Y_o + y_n Z_o) \\ &\quad + Ee(\sqrt{3}\, y_l + \sqrt{3}\, x_m - 3x_l - y_m)/2 \\ r_2^2 &= X_o^2 + Y_o^2 + Z_o^2 + E^2 + e^2 + 2e(y_l X_o + y_m Y_o + y_n Z_o) \\ &\quad - 2E(ey_m + Y_o) \\ r_3^2 &= X_o^2 + Y_o^2 + Z_o^2 + E^2 + e^2 + \sqrt{3}EX_o + EY_o \\ &\quad - \sqrt{3}e(x_l X_o + x_m Y_o + x_n Z_o) - e(y_l X_o + y_m Y_o + y_n Z_o) \\ &\quad - Ee(\sqrt{3}y_l + \sqrt{3}x_m + 3x_l + y_m)/2 \end{aligned} \tag{10}$$

Bring (5), (6), (8) and (9) into (10), it leads to:

$$\begin{aligned} r_1^2 &= \frac{1}{4c_\lambda^2}\left(3Ec_\alpha s_\lambda - \sqrt{3}Ec_\lambda + \sqrt{3}ec_\alpha\right)^2 \\ &\quad + \frac{1}{4}\left(es_\alpha s_\lambda - 2Z_0 + \sqrt{3}\, es_\alpha c_\lambda\right)^2 \\ r_2^2 &= (Z_0 + es_\alpha s_\lambda)^2 + \frac{1}{4}\left(3E - 3ec_\lambda + \sqrt{3}es_\lambda\right)^2 \\ &\quad + \frac{c_\alpha^2 s_\lambda^2}{4c_\lambda^2}\left(3E - 3ec_\lambda + \sqrt{3}es_\lambda\right)^2 \\ r_3^2 &= \frac{1}{4c_\lambda^2}\left(3Ec_\alpha s_\lambda + \sqrt{3}Ec_\lambda + \sqrt{3}ec_\alpha - 2\sqrt{3}ec_\alpha c_\lambda^2\right)^2 \\ &\quad + \frac{1}{4}\left(2Z_0 - es_\alpha s_\lambda + \sqrt{3}\, es_\alpha c_\lambda\right)^2 + 3e^2 s_\lambda^2 \end{aligned} \tag{11}$$

Equation (11) is the explicit inverse positional posture model of the proposed PM. According to (11), the inverse position solutions can be directly solved by the independent kinematic parameters ($\alpha$, $\lambda$ and $Z_o$) of $m$.

Eliminate $Z_o$ in (10), it leads to:

$$\begin{aligned} &3y_n(r_3^2 - r_1^2) - \sqrt{3}x_n(r_3^2 + r_1^2 - 2r_2^2) = 6\sqrt{3}E(y_n X_o - x_n Y_o) \\ &\quad - 3\sqrt{3}Ee(y_l y_n + x_m y_n) - 4\sqrt{3}Eey_m x_n \\ &\quad + \sqrt{3}\, Eex_n(3x_l + y_m) \\ &\quad - 6\sqrt{3}eX_o(x_l y_n - x_n y_l) - 6\sqrt{3}eY_o(x_m y_n - x_n y_m), \\ &\quad [r_1^2 + r_2^2 + r_3^2 - 3X_o^2 - 3Y_o^2 - 3E^2 - 3e^2 + 2Eey_m \\ &\quad + Ee(3x_l + y_m)]/3 \\ &= \{[6EY_o + 4Eey_m - Ee(3x_l + y_m) - r_3^2 - r_1^2 + 2r_2^2]/6ey_n \\ &\quad - y_l X_o/y_n - y_m Y_o/y_n\}^2 \end{aligned} \tag{12}$$

Since (12) contains many trigonometric functions, to simplify expression, let $t_1 = \tan(\alpha/2)$ and $t_2 = \tan(\gamma/2)$, then $s_\alpha = 2t_1/(1+t_1^2)$, $c_\alpha = (1 - t_1^2)/(1+t_1^2)$, $s_\gamma = 2t_2/(1+t_2^2)$ and $c_\gamma = (1 - t_2^2)/(1+t_2^2)$. Combined with (8) and (9), (12) can be simplified as below:

$$a_1 t_1^2 + a_2 = 0, \tag{13a}$$

$$b_1 t_1^6 + b_2 t_1^4 + b_3 t_1^2 + b_4 = 0 \tag{13b}$$

where $a_i (i = 1, 2)$ and $b_i (i = 1, 2, 3, 4)$ only contain $t_2$, which can be easily refined by MATLAB. Multiplying both sides of (13 a) by $t_1^2$ and $t_1^4$, respectively, it leads to:

$$\begin{aligned} a_1 t_1^4 + a_2 t_1^2 &= 0 \\ a_1 t_1^6 + a_2 t_1^4 &= 0 \end{aligned} \tag{14}$$

Since (13a), (13b) and (14) form a system of four linearly independent equations with four variables $t_1$, $t_1^2$, $t_1^4$ and $t_1^6$, it can be expressed in a matrix form as below:

$$\boldsymbol{Q}\begin{bmatrix} t_1^6 \\ t_1^4 \\ t_1^2 \\ 1 \end{bmatrix} = 0, \quad \boldsymbol{Q} = \begin{bmatrix} 0 & 0 & a_1 & a_2 \\ 0 & a_1 & a_2 & 0 \\ a_1 & a_2 & 0 & 0 \\ b_1 & b_2 & b_3 & b_4 \end{bmatrix} \tag{15}$$

where $\boldsymbol{Q}$ is a coefficient matrix of the above linear equations about $t_1$. Since $t_1$ must exist, there must be a nontrivial solution corresponding to (15). Based on the theory of linear algebra, it leads to:

$$|\boldsymbol{Q}| = 0 \tag{16}$$

Equation (16) is a nonlinear equation with only regard to $t_2$, which can be easily solved by MATLAB. After $t_2$ is

solved from (16), $t_1$ can be solved from (13a). Then, the independent kinematic parameters $\alpha$ and $\gamma$ corresponding to $t_1$ and $t_2$ can be obtained. Subsequently, the last one independent kinematic parameter $Z_o$ can be solved from (11).

Of course, the above forward positional posture model will get multiple solutions. However, combined with the computer-aided design variation geometry method [35], the unique solution can be determined.

### B. INVERSE VELOCITY MODEL

Denote $\boldsymbol{v_r}$ be the velocity vector of actuators and $\boldsymbol{V}$ be the velocity vector of $m$, respectively. For general $n$-DOF($n < 6$) non-over-constraint PM with linear active leg, $\boldsymbol{v_r}$ can be expressed as below [34]:

$$\begin{aligned}\begin{bmatrix} \boldsymbol{v}_r & n\times 1 \\ \boldsymbol{0}_{(6-n)\times 1} \end{bmatrix}_{6\times 1} &= \boldsymbol{J}_{6\times 6}\boldsymbol{V}_{6\times 1} \\ \boldsymbol{V}_{6\times 1} = \begin{bmatrix} \boldsymbol{v} \\ \boldsymbol{\omega} \end{bmatrix},\quad \boldsymbol{J}_{6\times 6} &= \begin{bmatrix} \boldsymbol{J}_{\boldsymbol{\alpha}} \\ \boldsymbol{J}_{\boldsymbol{v}} \end{bmatrix}, \\ \boldsymbol{J}_{\boldsymbol{\alpha}} = \begin{bmatrix} \boldsymbol{\delta}_1^{\mathrm{T}} & (\boldsymbol{e}_1\times\boldsymbol{\delta}_1)^{\mathrm{T}} \\ \vdots & \vdots \\ \boldsymbol{\delta}_n^{\mathrm{T}} & (\boldsymbol{e}_n\times\boldsymbol{\delta}_n)^{\mathrm{T}} \end{bmatrix}_{n\times 6} &\end{aligned} \tag{17}$$

where $\boldsymbol{J}$ is the Jacobian matrix which contains two sub-matrices, one is the traditional $n\times 6$ Jacobian matrix of limited-DOF PMs (named $\boldsymbol{J_\alpha}$), and the other one is the velocity constraints Jacobian matrix (named $\boldsymbol{J_v}$).

For this PM, since $F_{pi}$ ($i = 1, 2$) and $T_1$ do no work to $m$, it leads to:

$$\begin{aligned} &F_{p1}\boldsymbol{f}_1\cdot\boldsymbol{v} + (\boldsymbol{d}_1\times F_{p1}\boldsymbol{f}_1)\cdot\boldsymbol{\omega} = 0, \boldsymbol{d}_1 = \boldsymbol{A}_1 - \boldsymbol{O}' \\ &F_{p2}\boldsymbol{f}_2\cdot\boldsymbol{v} + (\boldsymbol{d}_2\times F_{p2}\boldsymbol{f}_2)\cdot\boldsymbol{\omega} = 0, \boldsymbol{d}_2 = \boldsymbol{C} - \boldsymbol{O}' \\ &T_1\boldsymbol{\tau}_1\cdot\boldsymbol{\omega} = 0 \end{aligned} \tag{18}$$

where $\boldsymbol{C}$ is the coordinate of $C$ in $\{O\text{-}XYZ\}$. Since $C$ is the intersection point of $R_{21}$ and $R_{24}$, $\boldsymbol{C}$ should meet $R_{21}$ and $R_{24}$ line equations simultaneously. From (3), the line equation of $R_{24}$ can be expressed as below:

$$\frac{(x - X_o)}{y_l} = \frac{(y - Y_o)}{y_m} = \frac{(z - Z_o)}{y_n} \tag{19}$$

Since the point on $R_{21}$ satisfies: $x = 0$ and $y = E$, substituting $x = 0$ and $y = E$ into (19), $\boldsymbol{C}$ can be derived.

$$C = \begin{bmatrix} 0 & E & Z_o + (E - Y_o)\dfrac{s_\alpha s_\lambda}{c_\lambda} \end{bmatrix} \tag{20}$$

Combined (4) with (18), it leads to:

$$\begin{aligned} &\begin{bmatrix} \boldsymbol{f}_1^T & (\boldsymbol{d}_1\times\boldsymbol{f}_1)^{\mathrm{T}} \\ \boldsymbol{f}_2^T & (\boldsymbol{d}_2\times\boldsymbol{f}_2)^{\mathrm{T}} \\ \boldsymbol{0} & \boldsymbol{\tau}_1^{\mathrm{T}} \end{bmatrix}\begin{bmatrix} \boldsymbol{v} \\ \boldsymbol{\omega} \end{bmatrix} = \boldsymbol{J_v}\boldsymbol{V} = \boldsymbol{0}, \\ &\boldsymbol{f}_1 = \begin{bmatrix} 0 & 1 & 0 \end{bmatrix}^{\mathrm{T}} \\ &\boldsymbol{f}_2 = \boldsymbol{R}_{22} = \frac{\boldsymbol{R}_{21}\times\boldsymbol{R}_{24}}{|\boldsymbol{R}_{21}\times\boldsymbol{R}_{24}|}, \\ &\boldsymbol{\tau}_1 = \frac{\boldsymbol{R}_{12}\times\boldsymbol{R}_{13}}{|\boldsymbol{R}_{12}\times\boldsymbol{R}_{13}|} = \boldsymbol{R}_{12}\times\boldsymbol{R}_{13} \end{aligned} \tag{21}$$

Then, combined (17) with (21), the inverse velocity model of the proposed PM is built:

$$\begin{aligned} \begin{bmatrix} \boldsymbol{v_r} \\ \boldsymbol{0}_{3\times 1} \end{bmatrix} = \boldsymbol{J}\begin{bmatrix} \boldsymbol{v} \\ \boldsymbol{\omega} \end{bmatrix},\quad \boldsymbol{J}_{6\times 6} &= \begin{bmatrix} \boldsymbol{\delta}_1^{\mathrm{T}} & (\boldsymbol{e}_1\times\boldsymbol{\delta}_1)^{\mathrm{T}} \\ \boldsymbol{\delta}_2^{\mathrm{T}} & (\boldsymbol{e}_2\times\boldsymbol{\delta}_2)^{\mathrm{T}} \\ \boldsymbol{\delta}_3^{\mathrm{T}} & (\boldsymbol{e}_3\times\boldsymbol{\delta}_3)^{\mathrm{T}} \\ \boldsymbol{f}_1^{\mathrm{T}} & (\boldsymbol{d}_1\times\boldsymbol{f}_1)^{\mathrm{T}} \\ \boldsymbol{f}_2^{\mathrm{T}} & (\boldsymbol{d}_2\times\boldsymbol{f}_2)^{\mathrm{T}} \\ 0 & \boldsymbol{\tau}_1^{\mathrm{T}} \end{bmatrix}, \\ \boldsymbol{v_r} &= \begin{bmatrix} v_{r1} \\ v_{r2} \\ v_{r3} \end{bmatrix} \end{aligned} \tag{22}$$

Since coupling relationships between the 6-dimensional positional posture of the moving platform are existed in limited-DOF PMs, there must exists velocity coupling relationships of the moving platform, which should be added to the inverse velocity model.

The relations between $\boldsymbol{V}$ and the velocity of independent kinematic parameters $\theta_i (i = 1, \ldots, n)$ for $n$-DOF($n < 6$) PMs can be expressed as below [34]:

$$\begin{aligned} \boldsymbol{v} &= \begin{bmatrix} v_x \\ v_y \\ v_z \end{bmatrix} = \boldsymbol{J}_{01}\dot{\theta}, \\ \boldsymbol{J}_{01} &= \begin{bmatrix} \dfrac{\partial X_o}{\partial\theta_1} & \dfrac{\partial X_o}{\partial\theta_2} & \cdots & \dfrac{\partial X_o}{\partial\theta_n} \\ \dfrac{\partial Y_o}{\partial\theta_1} & \dfrac{\partial Y_o}{\partial\theta_2} & \cdots & \dfrac{\partial Y_o}{\partial\theta_n} \\ \dfrac{\partial Z_o}{\partial\theta_1} & \dfrac{\partial Z_o}{\partial\theta_2} & \cdots & \dfrac{\partial Z_o}{\partial\theta_n} \end{bmatrix} \\ \boldsymbol{\omega} &= \begin{bmatrix} \omega_x \\ \omega_y \\ \omega_z \end{bmatrix} = \boldsymbol{J}_{02}\dot{\theta},\quad \boldsymbol{J}_{02} = \begin{bmatrix} \boldsymbol{R}_\alpha & \boldsymbol{R}_\beta & \boldsymbol{R}_\lambda \end{bmatrix} \\ &\times \begin{bmatrix} \dfrac{\partial\alpha}{\partial\theta_1} & \dfrac{\partial\alpha}{\partial\theta_2} & \cdots & \dfrac{\partial\alpha}{\partial\theta_n} \\ \dfrac{\partial\beta}{\partial\theta_1} & \dfrac{\partial\beta}{\partial\theta_2} & \cdots & \dfrac{\partial\beta}{\partial\theta_n} \\ \dfrac{\partial\lambda}{\partial\theta_1} & \dfrac{\partial\lambda}{\partial\theta_2} & \cdots & \dfrac{\partial\lambda}{\partial\theta_n} \end{bmatrix} \end{aligned} \tag{23}$$

where $\boldsymbol{J}_{01}$ and $\boldsymbol{J}_{02}$ are the linear and angular velocity decoupling Jacobian matrices, respectively.

For this PM, from (8) and (9), it leads to:

$$\boldsymbol{v} = \boldsymbol{J}_{01}\begin{bmatrix} \dot{\alpha} \\ \dot{\lambda} \\ \dot{Z}_o \end{bmatrix},\quad \boldsymbol{J}_{01} = \begin{bmatrix} \dfrac{\partial X_o}{\partial\alpha} & \dfrac{\partial X_o}{\partial\lambda} & \dfrac{\partial X_o}{\partial Z_o} \\ \dfrac{\partial Y_o}{\partial\alpha} & \dfrac{\partial Y_o}{\partial\lambda} & \dfrac{\partial Y_o}{\partial Z_o} \\ 0 & 0 & 1 \end{bmatrix} \tag{24}$$

Likewise, from (8) and (9), it leads to:

$$\boldsymbol{\omega} = \boldsymbol{R}_\alpha\dot{\alpha} + \boldsymbol{R}_\beta\dot{\beta} + \boldsymbol{R}_\lambda\dot{\lambda} = \begin{bmatrix} 0 & s_\alpha & 0 \\ 1 & 0 & 0 \\ 0 & c_\alpha & 0 \end{bmatrix}\begin{bmatrix} \dot{\alpha} \\ \dot{\lambda} \\ \dot{Z}_0 \end{bmatrix},$$

$$\boldsymbol{J}_{02}=\begin{bmatrix}0 & s_\alpha & 0\\ 1 & 0 & 0\\ 0 & c_\alpha & 0\end{bmatrix} \tag{25}$$

where:

$$\boldsymbol{R}_{\boldsymbol{\alpha}}=\begin{bmatrix}0\\1\\0\end{bmatrix},\quad \boldsymbol{R}_{\boldsymbol{\beta}}=\begin{bmatrix}c_\alpha\\0\\-s_\alpha\end{bmatrix},\quad \boldsymbol{R}_{\boldsymbol{\lambda}}=\begin{bmatrix}s_\alpha\\0\\c_\alpha\end{bmatrix}$$

Combination of (22), (24) and (25) are the explicit inverse velocity model of the proposed PM. When $\dot{\alpha}$, $\dot{\lambda}$ and $\dot{Z}_0$ are given, $\boldsymbol{V}$ can be obtained according to (24) and (25). Subsequently, $\boldsymbol{v_r}$ can be obtained according to (22).

### C. INVERSE ACCELERATION MODEL

Denote $\boldsymbol{a_r}$ be the acceleration vector of actuators and $\boldsymbol{A}$ be the acceleration vector of $m$. Deriving time from both sides of (17), $\boldsymbol{a}_r$ can be expressed as below:

$$\begin{bmatrix}\boldsymbol{a}_r\\ \boldsymbol{0}_{(6-n)\times 1}\end{bmatrix}=\boldsymbol{J}\boldsymbol{A}+\boldsymbol{V}^{\mathrm{T}}\boldsymbol{H}_{6\times6\times6}\boldsymbol{V},$$

$$\boldsymbol{A}=\begin{bmatrix}\boldsymbol{a}\\ \boldsymbol{\varepsilon}\end{bmatrix},\quad \boldsymbol{H}_{6\times6\times6}=\begin{bmatrix}\boldsymbol{H}_\alpha\\ \boldsymbol{H}_v\end{bmatrix}.$$

$$\boldsymbol{a}_r=\boldsymbol{J}_\alpha\boldsymbol{A}+\boldsymbol{V}^{\mathrm{T}}\boldsymbol{H}_\alpha\boldsymbol{V},\boldsymbol{H}_\alpha=\begin{bmatrix}\boldsymbol{H}_{\alpha1}\\ \boldsymbol{H}_{\alpha2}\\ \vdots\\ \boldsymbol{H}_{\alpha n}\end{bmatrix},$$

$$\boldsymbol{H}_{\alpha i}=\frac{1}{r_i}\begin{bmatrix}-\hat{\boldsymbol{\delta}}_i^2 & \hat{\boldsymbol{\delta}}_i^2\hat{\boldsymbol{e}}_i\\ -\hat{\boldsymbol{e}}_i\hat{\boldsymbol{\delta}}_i^2 & r_i\hat{\boldsymbol{e}}_i\hat{\boldsymbol{\delta}}_i+\hat{\boldsymbol{e}}_i\hat{\boldsymbol{\delta}}_i^2\hat{\boldsymbol{e}}_i\end{bmatrix}_{6\times6},$$

$$\boldsymbol{\sigma}=\begin{bmatrix}\sigma_x\\ \sigma_y\\ \sigma_z\end{bmatrix},\quad \hat{\boldsymbol{\sigma}}=\begin{bmatrix}0 & -\sigma_z & \sigma_y\\ \sigma_z & 0 & -\sigma_x\\ -\sigma_y & \sigma_x & 0\end{bmatrix} \tag{26}$$

where $\boldsymbol{H}$ is the Hessian matrix which contains two sub-matrices, one is the traditional Hessian matrix of limited–DOF PMs (named $\boldsymbol{H_\alpha}$), and the other one is the constraints Hessian matrix (named $\boldsymbol{H_v}$).

In order to solve $\boldsymbol{H_v}$, the derivatives of some vectors in (21) should be derived. For $r_1$:

$$\begin{aligned}\dot{\boldsymbol{f}}_1^{\mathrm{T}}&=\begin{bmatrix}0 & 0 & 0\end{bmatrix},\\ \dot{\boldsymbol{d}}_1^{\mathrm{T}}&=(\boldsymbol{\omega}\times\boldsymbol{d}_1)^{\mathrm{T}}=\left(-\hat{\boldsymbol{d}}_1\boldsymbol{\omega}\right)^{\mathrm{T}}=\boldsymbol{\omega}^{\mathrm{T}}\hat{\boldsymbol{d}}_1,\\ \left(\boldsymbol{d}_1\times\dot{\boldsymbol{f}}_1\right)^{\mathrm{T}}&=\left(\dot{\boldsymbol{d}}_1\times\boldsymbol{f}_1+\boldsymbol{d}_1\times\dot{\boldsymbol{f}}_1\right)^{\mathrm{T}}=\left(\boldsymbol{\omega}\times\boldsymbol{d}_1\times\boldsymbol{f}_1\right)^{\mathrm{T}}\\ &=\left(\hat{\boldsymbol{f}}_1\hat{\boldsymbol{d}}_1\boldsymbol{\omega}\right)^{\mathrm{T}}=\boldsymbol{\omega}^{\mathrm{T}}\hat{\boldsymbol{d}}_1\hat{\boldsymbol{f}}_1,\\ (\dot{\boldsymbol{\tau}}_1)^{\mathrm{T}}&=\left(\boldsymbol{R}_{12}\times\dot{\boldsymbol{R}}_{13}\right)^{\mathrm{T}}=\left(\dot{\boldsymbol{R}}_{12}\times\boldsymbol{R}_{13}+\boldsymbol{R}_{12}\times\dot{\boldsymbol{R}}_{13}\right)^{\mathrm{T}}\\ &=(\boldsymbol{R}_{12}\times(\boldsymbol{\omega}\times\boldsymbol{R}_{13}))^{\mathrm{T}}=-\boldsymbol{\omega}^{\mathrm{T}}\hat{\boldsymbol{Z}}'\hat{\boldsymbol{Y}}\end{aligned} \tag{27}$$

Based on the vector algorithm, $\boldsymbol{H_v}$ corresponding to $r_1$ can be expressed as below:

$$\begin{bmatrix}\dot{\boldsymbol{f}}_1^{\mathrm{T}} & \left(\boldsymbol{d}_1\times\dot{\boldsymbol{f}}_1\right)^{\mathrm{T}}\end{bmatrix}=\begin{bmatrix}\boldsymbol{v}^{\mathrm{T}} & \boldsymbol{\omega}^{\mathrm{T}}\end{bmatrix}\begin{bmatrix}\boldsymbol{0}_{3\times3} & \boldsymbol{0}_{3\times3}\\ \boldsymbol{0}_{3\times3} & \hat{\boldsymbol{d}}_1\hat{\boldsymbol{f}}_1\end{bmatrix}$$

$$\begin{bmatrix}\dot{\boldsymbol{0}}^{\mathrm{T}} & \dot{\boldsymbol{\tau}}_1^{\mathrm{T}}\end{bmatrix}=\begin{bmatrix}\boldsymbol{v}^{\mathrm{T}} & \boldsymbol{\omega}^{\mathrm{T}}\end{bmatrix}\begin{bmatrix}\boldsymbol{0}_{3\times3} & \boldsymbol{0}_{3\times3}\\ \boldsymbol{0}_{3\times3} & -\hat{\boldsymbol{Z}}'\hat{\boldsymbol{Y}}\end{bmatrix}$$

$$\boldsymbol{H}_{v1}=\begin{bmatrix}\boldsymbol{0}_{3\times3} & \boldsymbol{0}_{3\times3}\\ \boldsymbol{0}_{3\times3} & \hat{\boldsymbol{d}}_1\hat{\boldsymbol{f}}_1\end{bmatrix},$$

$$\boldsymbol{H}_{v3}=\begin{bmatrix}\boldsymbol{0}_{3\times3} & \boldsymbol{0}_{3\times3}\\ \boldsymbol{0}_{3\times3} & -\hat{\boldsymbol{Z}}'\hat{\boldsymbol{Y}}\end{bmatrix} \tag{28}$$

For $r_2$:

$$\begin{aligned}\dot{\boldsymbol{f}}_2&=\dot{\boldsymbol{R}}_{22}=\boldsymbol{\omega}_{22}\times\boldsymbol{R}_{22}=\dot{\theta}_{21}\boldsymbol{R}_{21}\times\boldsymbol{R}_{22}\\ &=\boldsymbol{R}_{21}\times\boldsymbol{R}_{22}\dot{\theta}_{21},\\ \left(\boldsymbol{d}_2\times\dot{\boldsymbol{f}}_2\right)^{\mathrm{T}}&=\left(\dot{\boldsymbol{d}}_2\times\boldsymbol{f}_2+\boldsymbol{d}_2\times\dot{\boldsymbol{f}}_2\right)^{\mathrm{T}}\\ &=\left(\dot{\boldsymbol{d}}_2\times\boldsymbol{f}_2+\boldsymbol{d}_2\times\left(\dot{\theta}_{21}\boldsymbol{R}_{21}\times\boldsymbol{R}_{22}\right)\right)^{\mathrm{T}}\end{aligned} \tag{29}$$

In order to get an explicit expression of (29), $\dot{\theta}_{21}$ and $\dot{\boldsymbol{d}}_2$ need to be solved. Considering $\omega$ is a composite of all $R$ joints in $r_2$, it leads to:

$$\boldsymbol{\omega}=\dot{\theta}_{21}\boldsymbol{R}_{21}+\dot{\theta}_{22}\boldsymbol{R}_{22}+\dot{\theta}_{23}\boldsymbol{R}_{23}+\dot{\theta}_{24}\boldsymbol{R}_{24} \tag{30}$$

To eliminate unnecessary parameters, dot multiply both side of (30) by $\boldsymbol{R}_{21}$ and $\boldsymbol{R}_{24}$, respectively, it leads to:

$$\begin{aligned}\boldsymbol{\omega}\cdot\boldsymbol{R}_{21}&=\dot{\theta}_{21}\boldsymbol{R}_{21}\cdot\boldsymbol{R}_{21}+\dot{\theta}_{22}\boldsymbol{R}_{22}\cdot\boldsymbol{R}_{21}+\dot{\theta}_{23}\boldsymbol{R}_{23}\cdot\boldsymbol{R}_{21}\\ &\quad+\dot{\theta}_{24}\boldsymbol{R}_{24}\cdot\boldsymbol{R}_{21},\\ \boldsymbol{\omega}\cdot\boldsymbol{R}_{24}&=\dot{\theta}_{21}\boldsymbol{R}_{21}\cdot\boldsymbol{R}_{24}+\dot{\theta}_{22}\boldsymbol{R}_{22}\cdot\boldsymbol{R}_{24}+\dot{\theta}_{23}\boldsymbol{R}_{23}\cdot\boldsymbol{R}_{24}\\ &\quad+\dot{\theta}_{24}\boldsymbol{R}_{24}\cdot\boldsymbol{R}_{24}\end{aligned} \tag{31}$$

Combined with (3) and (4), (31) can be reduced to the following form. Subsequently, $\dot{\theta}_{21}$ can be obtained:

$$\begin{aligned}&\boldsymbol{\omega}\cdot\boldsymbol{Z}=\dot{\theta}_{21}+\dot{\theta}_{24}\boldsymbol{Y}'\cdot\boldsymbol{Z},\quad \boldsymbol{\omega}\cdot\boldsymbol{Y}'=\dot{\theta}_{21}\boldsymbol{Z}\cdot\boldsymbol{Y}'+\dot{\theta}_{24}.\\ &\dot{\theta}_{21}=\frac{\left[\boldsymbol{Z}-\left(\boldsymbol{Y}'\cdot\boldsymbol{Z}\right)\boldsymbol{Y}'\right]}{1-\left(\boldsymbol{Y}'\cdot\boldsymbol{Z}\right)^2}\boldsymbol{\omega}\end{aligned} \tag{32}$$

In addition, considering $B_2A_2$, $B_2C$ and $CA_2$ are a closed-loop, it leads to:

$$\boldsymbol{B_2C}+\boldsymbol{CA_2}=\boldsymbol{B_2A_2} \tag{33}$$

Simultaneously derived time from both sides of (33), and let $v_{B_2C}$ and $v_{CA_2}$ be the velocity value of $\boldsymbol{B_2C}$ and $\boldsymbol{CA}_2$, respectively. It leads to:

$$\begin{aligned}&v_{B_2C}\boldsymbol{R}_{21}-v_{CA_2}\boldsymbol{R}_{24}+\boldsymbol{\omega}\times\boldsymbol{CA}_2=\boldsymbol{v}+\boldsymbol{\omega}\times\boldsymbol{e}_2\\ &v_{B_2C}\boldsymbol{R}_{21}-v_{CA_2}\boldsymbol{R}_{24}=\boldsymbol{v}+\boldsymbol{\omega}\times(\boldsymbol{e}_2-\boldsymbol{CA}_2)=\boldsymbol{v}+\boldsymbol{\omega}\times\boldsymbol{d}_2\end{aligned} \tag{34}$$

Meanwhile, $\dot{\boldsymbol{d}}_2$ can be derived. Combined with (34), it leads to:

$$\dot{d}_2=v_{cA2}\boldsymbol{R}_{24}+\boldsymbol{\omega}\times\boldsymbol{d}_2 \tag{35}$$

Since (35) still contains uncertainties parameters $v_{CA_2}$, dot multiply both sides of (34) by $\boldsymbol{X}$, it leads to:

$$\begin{aligned}&v_{B_2C}\boldsymbol{R}_{21}\cdot\boldsymbol{X}-v_{CA_2}\boldsymbol{R}_{24}\cdot\boldsymbol{X}=\boldsymbol{v}\cdot\boldsymbol{X}+(\boldsymbol{\omega}\times\boldsymbol{d}_2)\cdot\boldsymbol{X},\\ &-v_{CA_2}\boldsymbol{R}_{24}\cdot\boldsymbol{X}=\boldsymbol{v}\cdot\boldsymbol{X}+(\boldsymbol{\omega}\times\boldsymbol{d}_2)\cdot\boldsymbol{X},\end{aligned}$$

$$v_{CA_2} = -\frac{\boldsymbol{v}\cdot\boldsymbol{X} + (\boldsymbol{\omega}\times\boldsymbol{d}_2)\cdot\boldsymbol{X}}{\boldsymbol{R}_{24}\cdot\boldsymbol{X}} \tag{36}$$

From (32), (35) and (36), (29) can be expressed. Then, based on the vector algorithm, $\boldsymbol{H_v}$ corresponding to $r_2$ can be expressed as below (37), as shown at the bottom of the next page.

Combined with (26), (28) and (37), the inverse acceleration model of the proposed PM is established.

It is the same reason that there must exists acceleration coupling relationships of the moving platform, which should be added to the inverse acceleration model. Deriving time from both sides of (23), it leads to:

$$\begin{aligned}\boldsymbol{a} &= \boldsymbol{J}_{01}\ddot{\boldsymbol{\theta}} + \dot{\boldsymbol{J}}_{01}\dot{\boldsymbol{\theta}} = \boldsymbol{J}_{01}\ddot{\boldsymbol{\theta}} + \dot{\boldsymbol{\theta}}^{\mathrm{T}}\boldsymbol{H}_1\dot{\boldsymbol{\theta}}, \boldsymbol{H}_1 = \begin{bmatrix}\boldsymbol{H}_{11}\\ \boldsymbol{H}_{12}\\ \boldsymbol{H}_{13}\end{bmatrix}\\ \boldsymbol{\varepsilon} &= \boldsymbol{J}_{02}\ddot{\boldsymbol{\theta}} + \dot{\boldsymbol{J}}_{02}\dot{\boldsymbol{\theta}} = \boldsymbol{J}_{02}\ddot{\boldsymbol{\theta}} + \dot{\boldsymbol{\theta}}^{\mathrm{T}}\boldsymbol{H}_2\dot{\boldsymbol{\theta}}, \boldsymbol{H}_2 = \begin{bmatrix}\boldsymbol{H}_{21}\\ \boldsymbol{H}_{22}\\ \boldsymbol{H}_{23}\end{bmatrix}\end{aligned} \tag{38}$$

where:

$$\boldsymbol{H}_{11} = \begin{bmatrix} \frac{\partial^2 X_o}{\partial\theta_1\partial\theta_1} & \frac{\partial^2 X_o}{\partial\theta_2\partial\theta_1} & \cdots & \frac{\partial^2 X_o}{\partial\theta_n\partial\theta_1} \\ \frac{\partial^2 X_o}{\partial\theta_1\partial\theta_2} & \frac{\partial^2 X_o}{\partial\theta_2\partial\theta_2} & \cdots & \frac{\partial^2 X_o}{\partial\theta_n\partial\theta_2} \\ \vdots & \vdots & \cdots & \vdots \\ \frac{\partial^2 X_o}{\partial\theta_1\partial\theta_n} & \frac{\partial^2 X_o}{\partial\theta_2\partial\theta_n} & \cdots & \frac{\partial^2 X_o}{\partial\theta_n\partial\theta_n} \end{bmatrix},$$

$$\boldsymbol{H}_{12} = \begin{bmatrix} \frac{\partial^2 Y_o}{\partial\theta_1\partial\theta_1} & \frac{\partial^2 Y_o}{\partial\theta_2\partial\theta_1} & \cdots & \frac{\partial^2 Y_o}{\partial\theta_n\partial\theta_1} \\ \frac{\partial^2 Y_o}{\partial\theta_1\partial\theta_2} & \frac{\partial^2 Y_o}{\partial\theta_2\partial\theta_2} & \cdots & \frac{\partial^2 Y_o}{\partial\theta_n\partial\theta_2} \\ \vdots & \vdots & \cdots & \vdots \\ \frac{\partial^2 Y_o}{\partial\theta_1\partial\theta_n} & \frac{\partial^2 Y_o}{\partial\theta_2\partial\theta_n} & \cdots & \frac{\partial^2 Y_o}{\partial\theta_n\partial\theta_n} \end{bmatrix},$$

$$\boldsymbol{H}_{13} = \begin{bmatrix} \frac{\partial^2 Z_o}{\partial\theta_1\partial\theta_1} & \frac{\partial^2 Z_o}{\partial\theta_2\partial\theta_1} & \cdots & \frac{\partial^2 Z_o}{\partial\theta_n\partial\theta_1} \\ \frac{\partial^2 Z_o}{\partial\theta_1\partial\theta_2} & \frac{\partial^2 Z_o}{\partial\theta_2\partial\theta_2} & \cdots & \frac{\partial^2 Z_o}{\partial\theta_n\partial\theta_2} \\ \vdots & \vdots & \cdots & \vdots \\ \frac{\partial^2 Z_o}{\partial\theta_1\partial\theta_n} & \frac{\partial^2 Z_o}{\partial\theta_2\partial\theta_n} & \cdots & \frac{\partial^2 Z_o}{\partial\theta_n\partial\theta_n} \end{bmatrix},$$

$$\boldsymbol{H}_{2i} = \begin{bmatrix} \frac{\partial \boldsymbol{J}_{02}^{i1}}{\partial\theta_1} & \frac{\partial \boldsymbol{J}_{02}^{i2}}{\partial\theta_1} & \cdots & \frac{\partial \boldsymbol{J}_{02}^{in}}{\partial\theta_1} \\ \frac{\partial \boldsymbol{J}_{02}^{i1}}{\partial\theta_2} & \frac{\partial \boldsymbol{J}_{02}^{i2}}{\partial\theta_2} & \cdots & \frac{\partial \boldsymbol{J}_{02}^{in}}{\partial\theta_2} \\ \vdots & \vdots & \cdots & \vdots \\ \frac{\partial \boldsymbol{J}_{02}^{i1}}{\partial\theta_n} & \frac{\partial \boldsymbol{J}_{02}^{i2}}{\partial\theta_n} & \cdots & \frac{\partial \boldsymbol{J}_{02}^{in}}{\partial\theta_n} \end{bmatrix}$$

Here, $\boldsymbol{H}_1$ and $\boldsymbol{H}_2$ are the linear and angular acceleration decoupling Hessian matrices. $\boldsymbol{J}_{02}^{ij}$ denotes the elements in row $i$ and column $j$ of $\boldsymbol{J}_{02}$.

For this PM, from (9) and (24), it leads to:

$$\begin{aligned}\boldsymbol{a} &= \boldsymbol{J}_{01}\begin{bmatrix}\ddot{\alpha}\\ \ddot{\lambda}\\ \ddot{Z}_o\end{bmatrix} + \begin{bmatrix}\dot{\alpha} & \dot{\lambda} & \dot{Z}_o\end{bmatrix}\boldsymbol{H}_1\begin{bmatrix}\dot{\alpha}\\ \dot{\lambda}\\ \dot{Z}_o\end{bmatrix},\\ \boldsymbol{H}_1 &= \begin{bmatrix}\boldsymbol{H}_{11}\\ \boldsymbol{H}_{12}\\ \boldsymbol{H}_{13}\end{bmatrix},\\ \boldsymbol{H}_{11} &= \begin{bmatrix} \frac{\partial^2 X_o}{\partial\alpha\partial\alpha} & \frac{\partial^2 X_o}{\partial\lambda\partial\alpha} & 0 \\ \frac{\partial^2 X_o}{\partial\alpha\partial\lambda} & \frac{\partial^2 X_o}{\partial\lambda\partial\lambda} & 0 \\ 0 & 0 & 0 \end{bmatrix},\\ \boldsymbol{H}_{12} &= \begin{bmatrix} \frac{\partial^2 Y_o}{\partial\alpha\partial\alpha} & \frac{\partial^2 Y_o}{\partial\lambda\partial\alpha} & 0 \\ \frac{\partial^2 Y_o}{\partial\alpha\partial\lambda} & \frac{\partial^2 Y_o}{\partial\lambda\partial\lambda} & 0 \\ 0 & 0 & 0 \end{bmatrix},\\ \boldsymbol{H}_{13} &= \begin{bmatrix}0 & 0 & 0\\ 0 & 0 & 0\\ 0 & 0 & 0\end{bmatrix}\end{aligned} \tag{39}$$

Likewise, from (25), it leads to:

$$\begin{aligned}\boldsymbol{\varepsilon} &= \boldsymbol{J}_{02}\begin{bmatrix}\ddot{\alpha}\\ \ddot{\lambda}\\ \ddot{Z}_o\end{bmatrix} + \begin{bmatrix}\dot{\alpha} & \dot{\lambda} & \dot{Z}_o\end{bmatrix}\boldsymbol{H}_2\begin{bmatrix}\dot{\alpha}\\ \dot{\lambda}\\ \dot{Z}_o\end{bmatrix},\\ \boldsymbol{H}_2 &= \begin{bmatrix}\boldsymbol{H}_{21}\\ \boldsymbol{H}_{22}\\ \boldsymbol{H}_{23}\end{bmatrix}\end{aligned} \tag{40}$$

where:

$$\boldsymbol{H}_{21} = \begin{bmatrix}0 & c_\alpha & 0\\ 0 & 0 & 0\\ 0 & 0 & 0\end{bmatrix},\quad \boldsymbol{H}_{22} = \begin{bmatrix}0 & 0 & 0\\ 0 & 0 & 0\\ 0 & 0 & 0\end{bmatrix},$$

$$\boldsymbol{H}_{23} = \begin{bmatrix}0 & -s_\alpha & 0\\ 0 & 0 & 0\\ 0 & 0 & 0\end{bmatrix}$$

Combination of (26), (28), (37), (39) and (40) are the explicit inverse acceleration model of the proposed PM. When $\dot{\alpha}$, $\dot{\lambda}$, $\dot{Z}_0$, $\ddot{\alpha}$, $\ddot{\lambda}$ and $\ddot{Z}_0$ are given, $\boldsymbol{a}$ and $\varepsilon$ can be obtained according to (39) and (40). Subsequently, $\boldsymbol{a_r}$ can be obtained according to (26), (28) and (37).

## IV. STIFFNESS ANALYSIS OF THE RPU+UPU+SPU PM

### A. STATICS ANALYSIS AND CONSTRAINTS DECOMPOSITION

Utilizing the principle of static equilibrium, the relations between the active forces ($F_{ai}$) ($i = 1, 2, 3$), the constrained forces/torque ($F_{pi}/T_1$) ($i = 1, 2$) and the loading force/torque ($F/T$) can be expressed as below:

$$\begin{bmatrix}F_{a1} & F_{a2} & F_{a3} & F_{p1} & F_{p2} & T_1\end{bmatrix}^{\mathrm{T}} = -\left(\boldsymbol{J}_{6\times6}^{-1}\right)^{\mathrm{T}}\begin{bmatrix}\boldsymbol{F} & \boldsymbol{T}\end{bmatrix}^{\mathrm{T}} \tag{41}$$

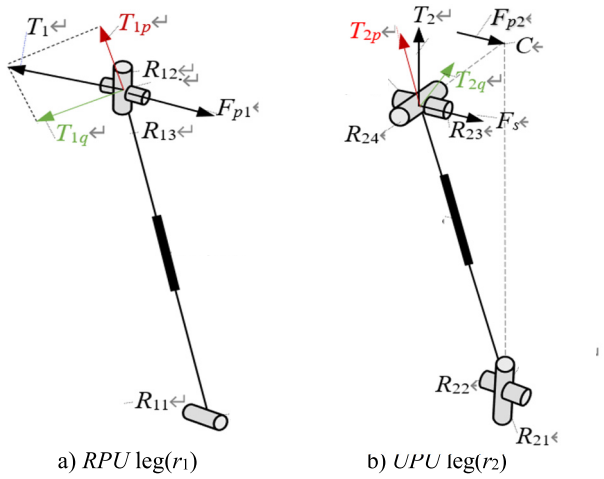


a) *RPU* leg($r_1$) b) *UPU* leg($r_2$)

**FIGURE 3. The constraints decomposition of $\mathbf{r_1}$ and $\mathbf{r_2}$.**

To find the wrenches directly causing deformations, $\boldsymbol{F}_{p2}$ should be decomposed [26]. Based on the principle of force equivalence, $\boldsymbol{F}_{p2}$ can be equivalent to a force $\boldsymbol{F_s}$ which is parallel with $\boldsymbol{F}_{p2}$ as well as passes through $A_2$ and a torque $\boldsymbol{T_2}$ which is perpendicular with $A_2C$ and $F_{p2}$. $\boldsymbol{F_s}$ and $\boldsymbol{T_2}$ can be expressed as below:

$$\begin{aligned}
&\boldsymbol{F}_s = \boldsymbol{F}_{p2}, \quad F_s = F_{p2}\\
&\boldsymbol{T}_2 = \boldsymbol{A_2C} \times \boldsymbol{F}_{p2} = (|\boldsymbol{A_2C}|\,\boldsymbol{R}_{24}) \times \left(F_{p2}\boldsymbol{R}_{23}\right)\\
&\quad = F_{p2}\,|\boldsymbol{A_2C}|\,(\boldsymbol{R}_{24} \times \boldsymbol{R}_{23}) \qquad (42)
\end{aligned}$$

To find the deformations due to $\boldsymbol{T}_i$, decompose $\boldsymbol{T}_i$ into two elements ($i = 1, 2$) [26], one is along $r_i$ (named $\boldsymbol{T_{ip}}$), and the other one is perpendicular to $r_i$ (named $\boldsymbol{T_{iq}}$), as shown in FIGURE 3. Let $\tau_2$, $\tau_{\boldsymbol{ip}}$ and $\tau_{\boldsymbol{iq}}$ be the unit vector of $\boldsymbol{T}_2$, $\boldsymbol{T}_{ip}$ and $\boldsymbol{T}_{iq}$, respectively. Based on (4), it leads to:

$$\begin{aligned}
&\boldsymbol{\tau}_{1p} = \boldsymbol{\delta}_1,\ \boldsymbol{\tau}_{1q} \perp \boldsymbol{\tau}_{1p},\ \boldsymbol{\tau}_{1p} \perp \boldsymbol{R}_{12},\ \boldsymbol{\tau}_1 \perp \boldsymbol{R}_{12},\ \boldsymbol{\tau}_{1q} \perp \boldsymbol{R}_{12},\\
&\boldsymbol{\tau}_{1q} = \boldsymbol{\delta}_1 \times \boldsymbol{R}_{12}\boldsymbol{\tau}_2 \perp \boldsymbol{R}_{23},\ \boldsymbol{\tau}_2 \perp \boldsymbol{R}_{24},\\
&\boldsymbol{\tau}_{2p} = \boldsymbol{\delta}_2,\ \boldsymbol{\tau}_{2q} \perp \boldsymbol{\tau}_{2p},\ \boldsymbol{\tau}_{2q} \perp \boldsymbol{R}_{23},\ \boldsymbol{\tau}_{2q} = \boldsymbol{\delta}_2 \times \boldsymbol{R}_{23} \qquad (43)
\end{aligned}$$

According to (43), the value of $\boldsymbol{T}_{ip}$ and $\boldsymbol{T}_{iq}$ ($i = 1, 2$) can be expressed as below:

$$\begin{aligned}
T_{1p} &= s_{1p}T_1, \quad s_{1p} = \boldsymbol{\tau}_1 \cdot \boldsymbol{\delta}_1\\
T_{1q} &= \left(\boldsymbol{\tau}_1 \cdot \boldsymbol{\tau}_{1q}\right) T_1 = s_{1q}T_1, \quad s_{1q} = \boldsymbol{\tau}_1 \cdot (\boldsymbol{\delta}_1 \times \boldsymbol{R}_{12})\\
T_{2p} &= \boldsymbol{T}_2 \cdot \boldsymbol{\tau}_{2p} = \boldsymbol{T}_2 \cdot \boldsymbol{\delta}_2 = F_{p2}\,|\boldsymbol{A_2C}|\,(\boldsymbol{R}_{24} \times \boldsymbol{R}_{23}) \cdot \boldsymbol{\delta}_2\\
&= s_{2p}F_{p2}\\
s_{2p} &= |\boldsymbol{A_2C}|\,(\boldsymbol{R}_{24} \times \boldsymbol{R}_{23}) \cdot \boldsymbol{\delta}_2\\
T_{2q} &= \boldsymbol{T}_2 \cdot \boldsymbol{\tau}_{2q} = \boldsymbol{T}_2 \cdot (\boldsymbol{\delta}_2 \times \boldsymbol{R}_{23})\\
&= F_{p2}\,|\boldsymbol{A_2C}|\,(\boldsymbol{R}_{24} \times \boldsymbol{R}_{23}) \cdot (\boldsymbol{\delta}_2 \times \boldsymbol{R}_{23}) = s_{2q}F_{p2}\\
s_{2q} &= |\boldsymbol{A_2C}|\,(\boldsymbol{R}_{24} \times \boldsymbol{R}_{23}) \cdot (\boldsymbol{\delta}_2 \times \boldsymbol{R}_{23}) \qquad (44)
\end{aligned}$$

where $s_{ip}/s_{iq}$ ($i = 1, 2$) is a coefficient representing the relationship between the constrained forces/torques and their components.

Though the above analysis, it leads to:

$$\begin{bmatrix} F_{a1}\\ F_{a2}\\ F_{a3}\\ F_{p1}\\ F_s\\ T_{1p}\\ T_{1q}\\ T_{2p}\\ T_{2q} \end{bmatrix} = \boldsymbol{W}_{9\times6} \begin{bmatrix} F_{a1}\\ F_{a2}\\ F_{a3}\\ F_{p1}\\ F_{p2}\\ T_1 \end{bmatrix},$$

$$\boldsymbol{W}_{9\times6} = \begin{bmatrix} 1 & 0 & 0 & 0 & 0 & 0\\ 0 & 1 & 0 & 0 & 0 & 0\\ 0 & 0 & 1 & 0 & 0 & 0\\ 0 & 0 & 0 & 1 & 0 & 0\\ 0 & 0 & 0 & 0 & 1 & 0\\ 0 & 0 & 0 & 0 & s_{2p} & 0\\ 0 & 0 & 0 & 0 & s_{2q} & 0\\ 0 & 0 & 0 & 0 & 0 & s_{1p}\\ 0 & 0 & 0 & 0 & 0 & s_{1q} \end{bmatrix} \qquad (45)$$

where $W$ is a coefficient matrix representing the relationship between the combination of the constrained wrenches and the active forces and the wrenches directly causing deformations.

$$\begin{bmatrix} \dot{f}_2^{\mathrm{T}} & \left(\boldsymbol{d}_2 \times \dot{\boldsymbol{f}}_2\right)^{\mathrm{T}} \end{bmatrix} = \begin{bmatrix} \boldsymbol{v}^{\mathrm{T}} & \boldsymbol{\omega}^{\mathrm{T}} \end{bmatrix} \times \begin{bmatrix} \boldsymbol{0}_{3\times3} & -\dfrac{\boldsymbol{X}\boldsymbol{R}_{24}^{\mathrm{T}}\hat{\boldsymbol{f}}_2}{\boldsymbol{R}_{24} \cdot \boldsymbol{X}}\\ \dfrac{\left[\boldsymbol{Z} - \left(\boldsymbol{Y}' \cdot \boldsymbol{Z}\right)\boldsymbol{y}\right](\boldsymbol{Z} \times f_2)^{\mathrm{T}}}{1 - \left(\boldsymbol{Y}' \cdot \boldsymbol{Z}\right)^2} & \left(\dfrac{-\hat{\boldsymbol{d}}_2\boldsymbol{X}\boldsymbol{R}_{24}^{\mathrm{T}}}{\boldsymbol{R}_{24} \cdot \boldsymbol{X}} + \hat{\boldsymbol{d}}_2\right)\hat{\boldsymbol{f}}_2 - \dfrac{\left[\boldsymbol{Z} - \left(\boldsymbol{Y}' \cdot \boldsymbol{Z}\right)\boldsymbol{y}\right](\boldsymbol{Z} \times f_2)^{\mathrm{T}}}{1 - \left(\boldsymbol{Y}' \cdot \boldsymbol{Z}\right)^2}\hat{\boldsymbol{d}}_2 \end{bmatrix}$$

$$\boldsymbol{H}_{v2} = \begin{bmatrix} \boldsymbol{0}_{3\times3} & -\dfrac{\boldsymbol{X}\boldsymbol{R}_{24}^{\mathrm{T}}\hat{\boldsymbol{f}}_2}{\boldsymbol{R}_{24} \cdot \boldsymbol{X}}\\ \dfrac{\left[\boldsymbol{Z} - \left(\boldsymbol{Y}' \cdot \boldsymbol{Z}\right)\boldsymbol{Y}'\right](\boldsymbol{Z} \times f_2)^{\mathrm{T}}}{1 - \left(\boldsymbol{Y}' \cdot \boldsymbol{Z}\right)^2} & \left(\dfrac{-\hat{\boldsymbol{d}}_2\boldsymbol{X}\boldsymbol{R}_{24}^{\mathrm{T}}}{\boldsymbol{R}_{24} \cdot \boldsymbol{X}} + \hat{\boldsymbol{d}}_2\right)\hat{\boldsymbol{f}}_2 - \dfrac{\left[\boldsymbol{Z} - \left(\boldsymbol{Y}' \cdot \boldsymbol{Z}\right)\boldsymbol{Y}'\right](\boldsymbol{Z} \times f_2)^{\mathrm{T}}}{1 - \left(\boldsymbol{Y}' \cdot \boldsymbol{Z}\right)^2}\hat{\boldsymbol{d}}_2 \end{bmatrix} \qquad (37)$$

### B. DEFORMATION ANALYSIS

Suppose that three elastic $r_i(i = 1, 2, 3)$ elastically suspend $m$ and all joints are a rigid body. Corresponding to different wrenches, deformations of $r_i$ can be analyzed based on the material mechanics.

a) The forces directly causing deformations:

$F_{ai}$ produces the longitudinal deformation $\delta_{ri}$ along $r_i(i = 1, 2, 3)$. Let $k_{ri}$ be a coefficient mapping the relationships of $\delta_{ri}$ and $F_{ai}$, it leads to:

$$F_{ai} = k_{ri}\delta_{ri}, k_{ri} = \frac{ES_i}{r_i} \tag{46}$$

where $E$ is the modular of elasticity and $S_i$ is the area of $r_i$.

$F_{p1}$ produces the flexibility deformations $\delta_{dp1}$ in $r_1$ and $F_s$ produces the flexibility deformations $\delta_{dp2}$ in $r_2$. Let $k_{p1}$ be a coefficient mapping the relationship of $\delta_{dp1}$ and $F_{p1}$, $k_{p2}$ be a coefficient mapping the relationship of $\delta_{dp2}$ and $F_s$, it leads to:

$$F_{p1} = k_{p1}\delta_{d_{p1}}, k_{p1} = \frac{3EI}{r_1^3}, \quad F_s = k_{p2}\delta_{d_{p2}}, k_{p2} = \frac{3EI}{r_2^3} \tag{47}$$

where $I$ is the moment inertia.

b) The torques directly causing deformations:

$T_{ip}$ produces the torsional deformation $\delta_{\theta ip}$ in $r_i(i = 1, 2)$. Let $k_{ip}$ be a coefficient mapping the relationships of $\delta_{\theta ip}$ and $T_{ip}$, it leads to:

$$T_{ip} = k_{ip}\delta_{\theta ip}, k_{ip} = \frac{GI_p}{r_i} \tag{48}$$

where $G$ is the shear modulus and $I_p$ is the polar moment of inertia.

$T_{iq}$ produces the bending deformation $\delta_{\theta iq}$ in $r_i(i = 1, 2)$. Let $k_{iq}$ be a coefficient mapping the relationships of $\delta_{\theta iq}$ and $T_{iq}$, it leads to:

$$T_{iq} = k_{iq}\delta\theta_{iq}, k_{iq} = \frac{EI}{r_i} \tag{49}$$

Though the above analysis, it leads to:

$$\begin{bmatrix} \boldsymbol{F}_a \\ \boldsymbol{F}_p \\ \boldsymbol{T}_1 \\ \boldsymbol{T}_2 \end{bmatrix} = \boldsymbol{K}^r_{9\times9} \begin{bmatrix} \delta\boldsymbol{r} \\ \delta\boldsymbol{d}_p \\ \delta\boldsymbol{\theta}_1 \\ \delta\boldsymbol{\theta}_2 \end{bmatrix}, \quad \boldsymbol{F}_a = \begin{bmatrix} F_{a1} \\ F_{a2} \\ F_{a3} \end{bmatrix},$$
$$\boldsymbol{F}_p = \begin{bmatrix} F_{p1} \\ F_s \end{bmatrix}, \quad \boldsymbol{T}_1 = \begin{bmatrix} T_{1p} \\ T_{1q} \end{bmatrix},$$
$$\boldsymbol{T}_2 = \begin{bmatrix} T_{2p} \\ T_{2q} \end{bmatrix}, \quad \delta\boldsymbol{r} = \begin{bmatrix} \delta r_1 \\ \delta r_2 \\ \delta r_3 \end{bmatrix},$$
$$\delta\boldsymbol{d}_p = \begin{bmatrix} \delta d_{p1} \\ \delta d_{p2} \end{bmatrix}, \quad \delta\boldsymbol{d}_1 = \begin{bmatrix} \delta\theta_{1p} \\ \delta\theta_{1q} \end{bmatrix}, \quad \delta\boldsymbol{\theta}_2 = \begin{bmatrix} \delta\theta_{2p} \\ \delta\theta_{2q} \end{bmatrix},$$
$$\boldsymbol{K}^r_{9\times9} = diag(k_{r1}, k_{r2}, k_{r3}, k_{p1}, k_{p2}, k_{1p}, k_{1q}, k_{2p}, k_{2q}) \tag{50}$$

where $\boldsymbol{K}^r$ is a coefficient matrix mapping the relationships between the deformations and the wrenches directly causing deformations.

### C. STIFFNESS MODEL

Let $\delta\boldsymbol{p} = [\delta x\delta y\delta z]^{\mathrm{T}}$, $\delta\ \Phi = [\delta\Phi_x\delta\Phi_y\delta\Phi_z]^{\mathrm{T}}$ be the linear and angular deformations of $m$. According to the principle of virtue work, it leads to:

$$[\boldsymbol{F}_a^{\mathrm{T}} \quad \boldsymbol{F}_p^{\mathrm{T}} \quad \boldsymbol{T}_1^{\mathrm{T}} \quad \boldsymbol{T}_2^{\mathrm{T}}] \begin{bmatrix} \delta\boldsymbol{r} \\ \delta\boldsymbol{d}_p \\ \delta\boldsymbol{\theta}_1 \\ \delta\boldsymbol{\theta}_2 \end{bmatrix} = -[\boldsymbol{F}^{\mathrm{T}} \quad \boldsymbol{T}^{\mathrm{T}}] \begin{bmatrix} \delta\boldsymbol{p} \\ \delta\boldsymbol{\psi} \end{bmatrix} \tag{51}$$

Substituting (45) into (51), and combining with (41), it leads to:

$$(\boldsymbol{W}_{9\times6} \begin{bmatrix} F_{a1} \\ F_{a2} \\ F_{a3} \\ F_{p1} \\ F_{p2} \\ T_1 \end{bmatrix})^{\mathrm{T}} \begin{bmatrix} \delta\boldsymbol{r} \\ \delta\boldsymbol{d}_p \\ \delta\boldsymbol{\theta}_1 \\ \delta\boldsymbol{\theta}_2 \end{bmatrix} = \begin{bmatrix} F_{a1} \\ F_{a2} \\ F_{a3} \\ F_{p1} \\ F_{p2} \\ T_1 \end{bmatrix}^{\mathrm{T}} \boldsymbol{W}^{\mathrm{T}}_{9\times6} \begin{bmatrix} \delta\boldsymbol{r} \\ \delta\boldsymbol{d}_p \\ \delta\boldsymbol{\theta}_1 \\ \delta\boldsymbol{\theta}_2 \end{bmatrix}$$
$$= -\left[\boldsymbol{F}^{\mathrm{T}}\ \boldsymbol{T}^{\mathrm{T}}\right]\boldsymbol{J}^{-1}_{6\times6}\boldsymbol{W}^{\mathrm{T}}_{9\times6} \begin{bmatrix} \delta\boldsymbol{r} \\ \delta\boldsymbol{d}_p \\ \delta\boldsymbol{\theta}_1 \\ \delta\boldsymbol{\theta}_2 \end{bmatrix} = -\left[\boldsymbol{F}^{\mathrm{T}} \quad \boldsymbol{T}^{\mathrm{T}}\right] \begin{bmatrix} \delta\boldsymbol{p} \\ \delta\boldsymbol{\psi} \end{bmatrix} \tag{52}$$

According to (52), the deformation relations can be derived as below:

$$\begin{bmatrix} \delta\boldsymbol{p} \\ \delta\boldsymbol{\Phi} \end{bmatrix} = \boldsymbol{J}^{-1}_{6\times6}\boldsymbol{W}^{\mathrm{T}}_{6\times6} \begin{bmatrix} \delta\boldsymbol{r} \\ \delta\boldsymbol{d}_p \\ \delta\boldsymbol{\theta}_1 \\ \delta\boldsymbol{\theta}_2 \end{bmatrix} \tag{53}$$

Furthermore, from (41), (45) and (53), it leads to:

$$\begin{bmatrix} \delta\boldsymbol{r} \\ \delta\boldsymbol{d}_p \\ \delta\boldsymbol{\theta}_1 \\ \delta\boldsymbol{\theta}_2 \end{bmatrix} = -\boldsymbol{C}^r_{9\times9}\boldsymbol{W}_{9\times6}\left(\boldsymbol{J}^{-1}_{6\times6}\right)^{\mathrm{T}} \begin{bmatrix} \boldsymbol{F} \\ \boldsymbol{T} \end{bmatrix}, \quad \boldsymbol{C}^r_{9\times9} = \left(\boldsymbol{K}^r_{9\times9}\right)^{-1} \tag{54}$$

Substituting (54) into (53), it leads to:

$$\begin{bmatrix} \delta\boldsymbol{p} \\ \delta\boldsymbol{\Phi} \end{bmatrix} = -\boldsymbol{C}_{6\times6} \begin{bmatrix} \boldsymbol{F} \\ \boldsymbol{T} \end{bmatrix},$$
$$\boldsymbol{C}_{6\times6} = -\boldsymbol{J}^{-1}_{6\times6}\boldsymbol{W}^{\mathrm{T}}_{9\times6}\boldsymbol{C}^r_{9\times9}\boldsymbol{W}_{9\times6}(\boldsymbol{J}^{-1}_{6\times6})^{\mathrm{T}} \tag{55}$$

From (55), the stiffness model of the proposed PM is built:

$$\begin{bmatrix} \boldsymbol{F} \\ \boldsymbol{T} \end{bmatrix} = \boldsymbol{K}_{6\times6} \begin{bmatrix} \delta\boldsymbol{p} \\ \delta\boldsymbol{\Phi} \end{bmatrix}, \quad \boldsymbol{K}_{6\times6} = -\boldsymbol{C}_{6\times6} \tag{56}$$

where $\boldsymbol{K}_{6\times6}$ and $\boldsymbol{C}_{6\times6}$ is the stiffness matrix and compliance matrix of this PM, respectively.

## V. NUMERICAL EXAMPLES

The correctness of the previously established models is verified in this section.

### A. FORWARD POSITIONAL POSTURE NUMERICAL EXAMPLE

For this example PM, the dimension parameters and the active parameters of each leg are shown in TABLE 1.

**TABLE 1. The dimension parameters and the ACTIVE parameters of each leg for this example PM.**

| The dimension parameters | | The active parameters of each leg | | |
|---|---|---|---|---|
| $E$(cm) | $e$(cm) | $r_1$(cm) | $r_2$ (cm) | $r_3$ (cm) |
| 60 | 40 | 165 | 162 | 163 |

According to TABLE 1, (15) can be written in a specific expression and $\boldsymbol{Q}$ can be obtained. Then $t_2$ can be solved form (16), the detailed values are listed in TABLE 2. In order to determine the acceptable analytic solution from TABLE 2, the simulative PM is created using the computer-aided design variation geometry method [35], as shown in FIGURE 4.

**TABLE 2. The 28 solutions of t2.**

| No. | Values | | | |
|---|---|---|---|---|
| 1-4 | −2.4730 | −0.2774 | −0.2297 | −0.1389 |
| 5-8 | 0.1612 | 0.1998 | 0.2272 | 1.152 |
| 9-12 | −1.236 + 0.8929i | −1.236−0.8929i | $-1.0 + 4.022\times10^{-9}$i | $-1.0 - 4.022\times10^{-9}$i |
| 13-16 | −0.5924−0.8835i | −0.5924 + 0.8835i | −0.3875−0.6176i | −0.3875+0.6176i |
| 17-20 | $1.971\times10^{-18}$−1.0i | $1.971\times10^{-18}$ + 1.0i | $2.251\times10^{-16}$+$1.37\times10^{-8}$i | $2.251\times10^{-16}$−$1.37\times10^{-8}$i |
| 21-24 | 0.8374−1.074i | 0.8374+1.074i | 1.0−7.696×10−9i | $1.0+7.696\times10^{-9}$i |
| 25-28 | 4.117−16.66i | 4.117+16.66i | $15.57+3.107\times10^{8}$i | $15.57-3.107\times10^{8}$i |

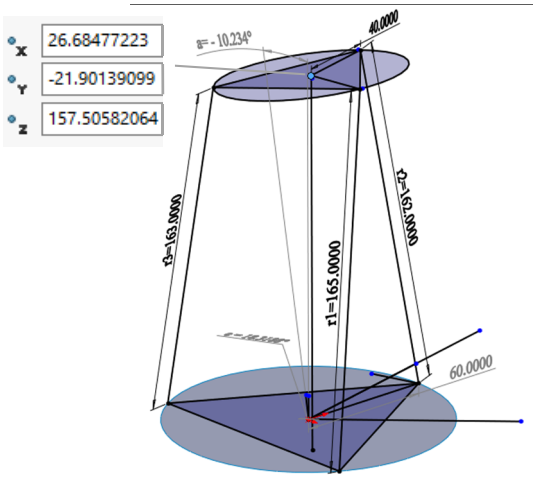


**FIGURE 4. The simulative model for this example PM.**

In the CAD software when given the identical settings of TABLE 1 to the simulative PM, the value of λ can be measured, which is in excellent agreement with the 5th solution in TABLE 2. Subsequently, bring the 5th solution $t_2 = 0.1612$ (corresponding to $\lambda = 18.3146$) into (9), (11) and (13a), other positional posture parameters can be solved. The detailed analytic values are shown in TABLE 3.

Meanwhile, the simulative value of the positional posture parameters can be measured form the simulative PM, the detailed simulative values are shown in TABLE 3. From TABLE 3, it can be seen that the analytic values and the

**TABLE 3. Comparison of the values between analytic and simulative.**

| Parameters | Analytic Values | Simulation Values | Parameters | Analytic Values | Simulation Values |
|---|---|---|---|---|---|
| $X_o$(cm) | 26.6848 | 26.68477223 | $\alpha$ | −10.2287 | −10.23400467 |
| $Y_o$(cm) | −21.9014 | −21.90139099 | $\beta$ | 0 | 0 |
| $Z_o$(cm) | 157.5058 | 157.50582064 | $\lambda$ | 18.3146 | 18.31884416 |

**TABLE 4. The initial independent motion parameters and their acceleration.**

| INITIAL | | | ACCELERATION | | |
|---|---|---|---|---|---|
| $a$ (°) | $\lambda$ (°) | $Z_0$ (m) | $\ddot{\alpha}$ (°/s$^2$) | $\ddot{\lambda}$ (°/s$^2$) | $\ddot{Z}_0$ (m/s$^2$) |
| -21 | 21 | 1.60 | Sin((π/4) × t) | Sin((π/3) × t) | 0.6×t |

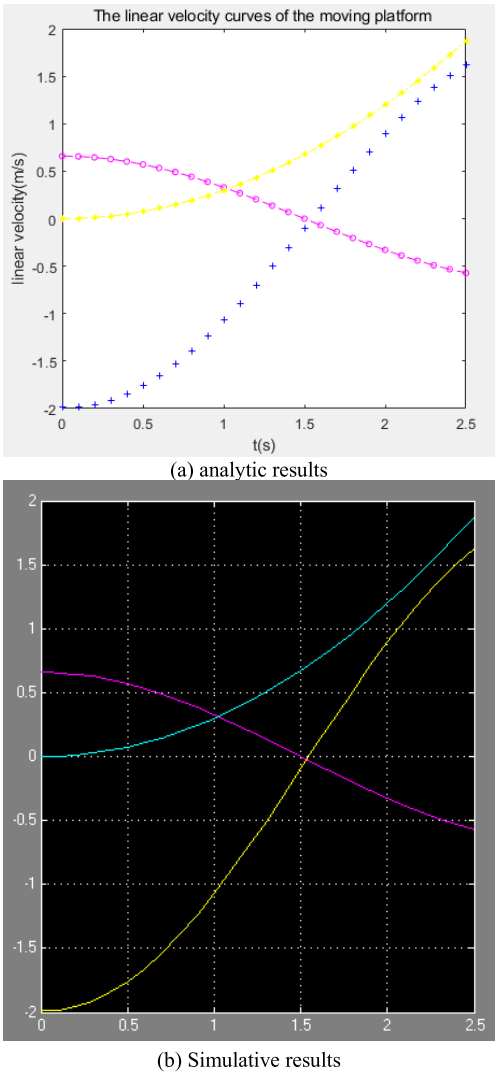


(a) analytic results

(b) Simulative results

**FIGURE 5. The comparison of simulative and analytic results about linear velocity of *m*.**

**TABLE 5. The comparison of simulative and analytic values about kinematic.**

| Kinematic | $t$=0.5s | | $t$=1.5s | | $t$=2.5s | |
|---|---|---|---|---|---|---|
| Parameters | Analytic | Simulative | Analytic | Simulative | Analytic | Simulative |
| $v_x$ | -1.7595 | -1.7595 | -0.0964 | $-9.6350\times10^{-2}$ | 1.6256 | 1.6256 |
| $v_y$ | 0.5709 | 0.057094 | 0 | 0 | -0.5709 | -0.57094 |
| $v_z$ | 0.0750 | $7.5000\times10^{-2}$ | 0.6750 | 0.67500 | 1.8750 | 1.8750 |
| $\omega_x$ | 0.0050 | $5.0264\times10^{-3}$ | 0 | 0 | -0.0048 | $-4.8186\times10^{-3}$ |
| $\omega_y$ | -0.0205 | $-2.0531\times10^{-2}$ | -0.0085 | $-8.5041\times10^{-3}$ | 0.0085 | $8.5041\times10^{-3}$ |
| $\omega_z$ | -0.0135 | $-1.3530\times10^{-2}$ | 0 | 0 | 0.0136 | $1.3606\times10^{-2}$ |
| $a_x$ | 1.0412 | 1.0412 | 2.0551 | 2.0551 | 1.1443 | 1.1443 |
| $a_y$ | -0.3464 | -0.34643 | -0.6912 | -0.69119 | -0.3464 | -0.34643 |
| $a_z$ | 0.3000 | 0.3000 | 0.9000 | 0.9000 | 1.5000 | 1.5000 |
| $\varepsilon_x$ | -0.0028 | $-2.7612\times10^{-3}$ | -0.0058 | $-5.8267\times10^{-3}$ | -0.0028 | $-2.7976\times10^{-3}$ |
| $\varepsilon_y$ | 0.0067 | $6.6791\times10^{-3}$ | 0.0161 | $1.6125\times10^{-2}$ | 0.0161 | $1.1625\times10^{-2}$ |
| $\varepsilon_z$ | 0.0083 | $8.2836\times10^{-3}$ | 0.0165 | $1.6452\times10^{-2}$ | 0.0083 | $8.267\times10^{-3}$ |

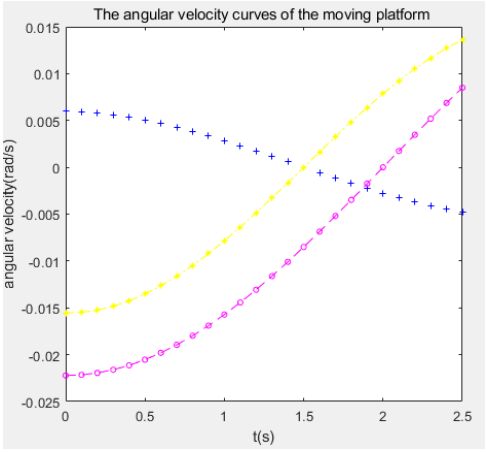


(a) analytic results

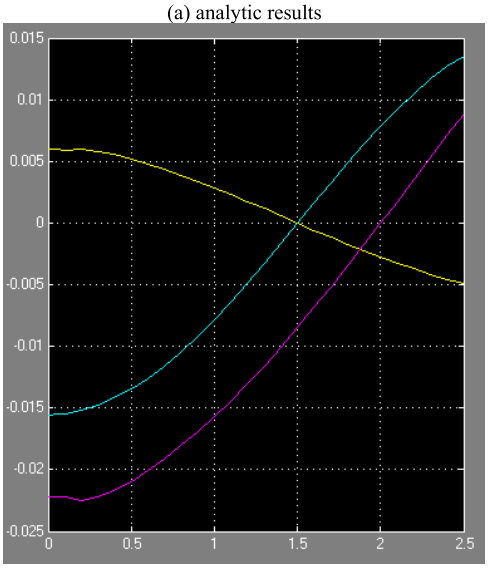

(b) Simulative results

**FIGURE 6. The comparison of simulative and analytic results about angular velocity of *m*.**

simulative values are very close, which shows the forward positional posture model established in this study is accurate.

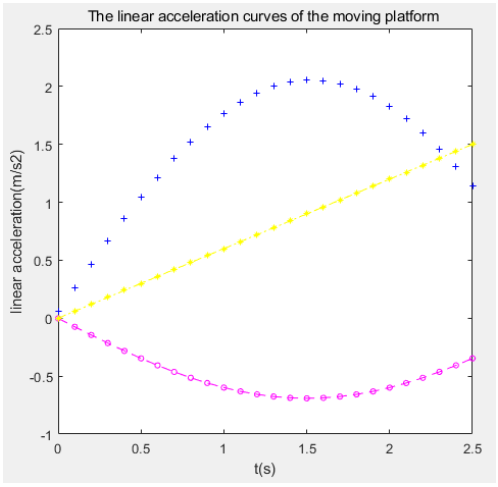


(a) analytic results

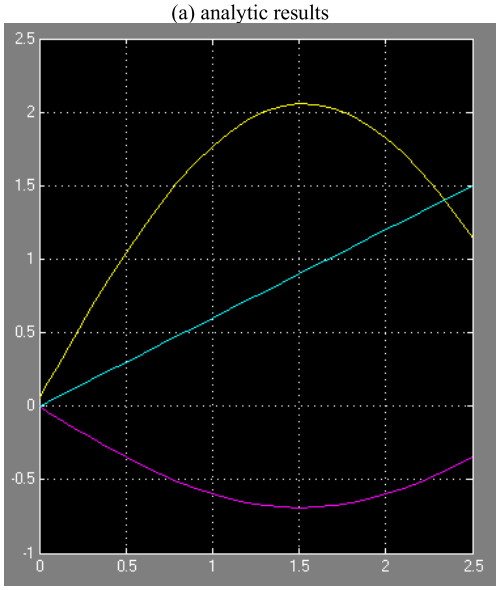

(b) Simulative results

**FIGURE 7. The comparison of simulative and analytic results about linear acceleration of *m*.**

### *B. KINEMATIC NUMERICAL EXAMPLE*

For this example PM, set $E = 0.60$m and $e = 0.40$m. Meanwhile let the independent motion parameters move according to the items in TABLE 4.

From an analytic point of view, when motions of the independent motion parameters are given, the initial positional posture of $m$ can be calculated based on (9). The velocity $\boldsymbol{v}$ and $\boldsymbol{\omega}$ of $m$ can be calculated based on (24) and (25), FIGURE 5(a) and 6(a) shows the corresponding analytic values curves plotted by MATLAB.

The acceleration a and $\varepsilon$ of m can be calculated based on (39) and (40), FIGURE 7(a) and 8(a) shows the corresponding analytic values curves plotted by MATLAB. Furthermore, according to the above expected motions of $m$, the initial length of actuators can be calculated based on (11). $v_{ri}$ (i = 1, 2, 3) can be calculated based on (22).

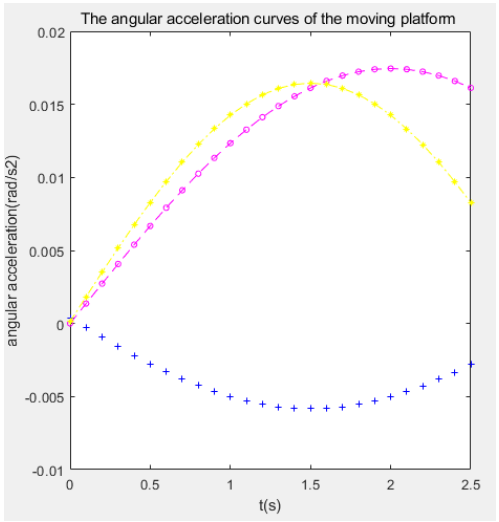


(a) analytic results

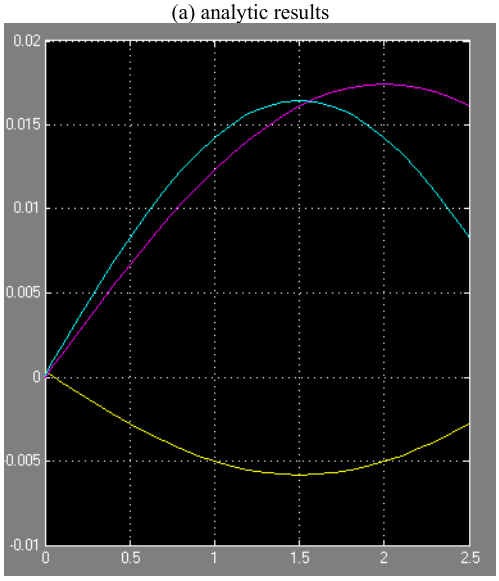

(b) Simulative results

**FIGURE 8.** **The comparison of simulative and analytic results about angular acceleration.**

And $a_{ri}$ (i = 1, 2, 3) can be calculated based on (26), (28) and (37).

From a simulative point of view, a simulative PM by MATLAB/SIMULINK is set, as shown in FIGURE 9. In the simulative PM, three simulation-driven modules are set on $r_i$ ($i$ = 1, 2, 3), a velocity/acceleration sensor is set on $m$ and the sensor values can display by scope. Appling identical $v_{ri}$, $a_{ri}$ calculated above to the corresponding simulation-driven module, the scope displays the corresponding simulative values curves, as shown in FIGURE 5,6,7, and 8 (b).

The quantitative comparisons between the analytic values and the simulative values at t= 0s, t= 1.25s, t= 2.5s are shown in TABLE 5.

By comparing the curves in FIGURE 5,6,7 and 8 and the values in TABLE 5, it can be seen that the analytic values and the simulative values are in excellent agreement, which

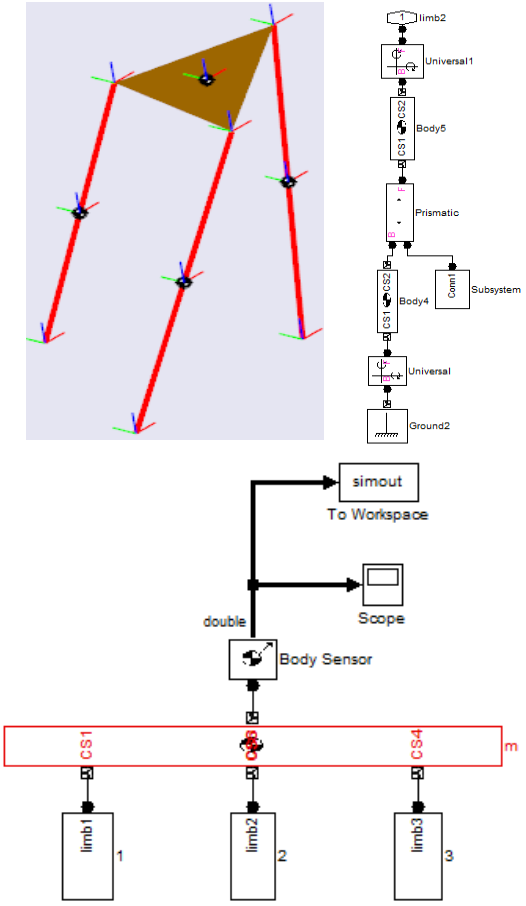


**FIGURE 9.** **Simulative mechanism of the RPU+UPU+SPU PM.**

**TABLE 6.** **The dimension parameters, the initial independent motion parameters and the mechanical parameters of materials.**

| The dimension parameters | | The initial independent motion parameters | | | Load | |
|---|---|---|---|---|---|---|
| $E$(m) | $e$(m) | $\alpha$(°) | $\lambda$(°) | $Z_0$(m) | $\boldsymbol{F}_0$(N) | $\boldsymbol{T}_0$(N/s) |
| $1.20/\sqrt{3}$ | $0.60/\sqrt{3}$ | -18.62 | 12.4 | 1.36 | $[5\ 10\ 10]^T$ | $[0\ 0\ 0]^T$ |
| The mechanical parameters of materials | | | | | | |
| $E$(Pa) | $E_I$(N·m$^2$) | $A$(m$^2$) | | $G$(Pa) | | $I_p$(m$^4$) |
| $2.11\times10^{11}$ | 26502 | 0.0013 | | $80\times10^9$ | | $2.5120\times10^{-7}$ |

**TABLE 7.** **The comparison of simulative and analytic values about the deformations of *m*.**

| Elastic deformation of $m$ | $\delta x$ (m) | $\delta y$(m) | $\delta z$(m) |
|---|---|---|---|
| analytics results | $-0.4650\times10^{-3}$ | $0.7764\times10^{-3}$ | $0.2580\times10^{-3}$ |
| FE model results | $-0.5230\times10^{-3}$ | $0.8165\times10^{-3}$ | $0.3293\times10^{-3}$ |

verifies the correctness and precision of the kinematic model established in this study.

### C. STIFFNESS NUMERICAL EXAMPLE

For this example PM, the dimension parameters, the initial independent motion parameters, the load force/torque and the mechanical parameters of materials are shown in TABLE 6.

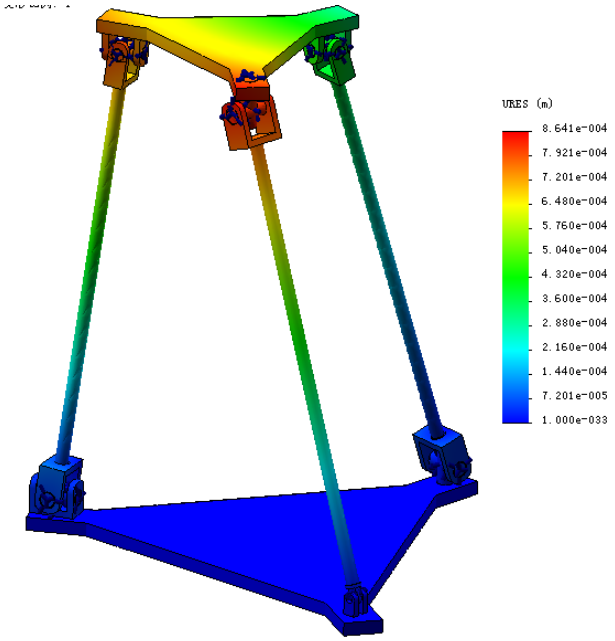


**FIGURE 10.** The elastic deformations of the EF model.

From an analytic point of view, in the state shown in TABLE 6, $\boldsymbol{J}_{6\times6}$ can be determined by (22), $\boldsymbol{W}_{9\times6}$ can be determined by (45), $\boldsymbol{C}_{9\times9}$ can be determined by (50). Then the stiffness matrix $\boldsymbol{K}$ can be calculated according to (55) the equation can be derived, as shown at the top of next page.

Subsequently, the deformations of $m$ can be calculated according to (56). The detailed analytic values are shown in TABLE 7.

From a simulative point of view, a finite element simulative model is established by SolidWorks according to the dimension and material parameters described in TABLE 6. When applying the identical wrenches as the analytic model to the finite element simulative model, the deformations can be obtained, as shown in FIGURE 10. The detailed simulative values are shown in TABLE 7.

Since the results of the FE simulated model depend on multiple key factors (e. g. dimensions and types, boundary constraints, solver, connection constraints), it is well known that the results of the FE model are approximate numerical results. Therefore, the analytic deformation values and the simulative deformation values in TABLE 6 are basically coincident, which is acceptable for stiffness analysis, and verifies the correctness of the stiffness model established in this study.

In future work, a *RPU+UPU+SPU* machine tools prototype will be designed and fabricated, and the experimental study will be performed to further validate the correctness of the kinematic and stiffness models built in this study.

## VI. CONCLUSION

This study proposes a novel asymmetric non-over-constraint 3-DOF *RPU+UPU+SPU* PM.

The complete kinematic models for the *RPU+UPU+SPU* PM are built. Simulative PMs are set to validate the accuracy of the conducted kinematic models.

A 6 × 6 form Jacobian matrix is derived. And a 6 × 6 × 6 form Hessian matrix is derived. The velocity/ acceleration coupling relationships of the moving platform are derived to supplement the inverse kinematic models.

Both considering the active forces and the constraint wrenches, the stiffness model of the *RPU+UPU+SPU* PM are established.

The stiffness matrix and compliance matrix are derived. A FE simulative PM is built to validate the accuracy of the conducted stiffness model.

## APPENDIX

## SYMBOL TABLE

| Symbol | Meaning |
|---|---|
| *R, P, U* and *S* | The revolute joint, the prismatic joint, the universal joint, and the sphere joint, |
| $M$ | The DOF number of the mechanism |
| $n$ | The number of links in the mechanism |
| $g$ | The number of joints |
| $m_i$ | The DOF number of the $i$-th joint |
| $m_0$ | The passive DOF |
| $B_1$, $B_2$ and $B_3$ | The vertex of the base platform |
| $\boldsymbol{B_i}$ | The vector of vertex $B_i$ in the inertial frame *O-XYZ* |
| *O-XYZ* | The coordinate axes of the inertial frame |
| $\boldsymbol{X}$, $\boldsymbol{Y}$ and $\boldsymbol{Z}$ | The unit vector of axes $X$, $Y$, $Z$ |
| $E$ | The distance from origin $O$ to vertex $B_i$ |
| $A_1$, $A_2$ and $A_3$ | The vertex of the moving platform |
| $\boldsymbol{A_i}$ | The vector of vertex $A_i$ in the inertial frame *O-XYZ* |
| ${}^{m}\boldsymbol{A_i}$ | The vector of vertex $A_i$ in the frame $O'$ $X'$ $Y'$ $Z'$ |
| $O'$ -$X'$ $Y'$ $Z'$ | The coordinate axes of the moving frame |
| $\boldsymbol{X'}$, $\boldsymbol{Y'}$ and $\boldsymbol{Z'}$ | The unit vector of axes $X'$, $Y'$, $Z'$ |
| $e$ | The distance from origin $O'$ to vertex $A_i$. |
| ${}^{B}_{m}\boldsymbol{R}$ | The rotational transformation matrix from frame $O'$ -$X'$ $Y'$ $Z'$to inertial frame *O-XYZ* |
| $R_{ij}$, $\boldsymbol{R}_{ij}$ | The $j$-th $R$ joint from the base platform to the moving platform in the $i$-th leg, the unit vector of $R_{ij}$ |
| $r_i$, $\boldsymbol{\delta_i}$ | The length of the $i$-th leg, the unit vector of $r_i$ |
| $F_{p1}$ and $T_p$ | The constrained force and torque in the 1st leg |
| $F_{p2}$ | The constrained force in the 2nd leg |
| $\boldsymbol{f_i}$ and $\tau$ | The unit vectors of $\boldsymbol{F_{pi}}(i = 1,2)$ and $\boldsymbol{T_P}$ |
| $C$, $\boldsymbol{C}$ | The action point of $F_{p1}$, the coordinate of point $C$ in the inertial frame O-XYZ |
| $\boldsymbol{e_i}$ | The vector from origin $O'$ to vertex $A_i$ |
| $\boldsymbol{d_i}$ | The vector from origin $O'$ to the action point of $F_{pi}$ |
| $\boldsymbol{O'}$ | The vectors of origin $O'$ in the inertial frame *O-XYZ* |

$$\boldsymbol{K}_{6\times6} = \begin{bmatrix} -0.3157 & 0.1309 & -0.7097 & 0.1080 & -0.1874 & -0.0864 \\ 0.1309 & -0.3138 & 0.8263 & 0.1799 & 0.0786 & 0.0199 \\ -0.7097 & 0.8263 & -4.8755 & 0.0814 & 0.1445 & -0.1866 \\ 0.1080 & 0.1799 & 0.0814 & -0.2730 & -0.0143 & 0.0467 \\ -0.1874 & 0.0786 & 0.1445 & -0.0143 & -0.2585 & -0.0449 \\ -0.0864 & 0.0199 & -0.1866 & 0.0467 & -0.0449 & -0.0251 \end{bmatrix} \times 10^8$$

| | |
|---|---|
| $X_o$, $Y_o$ and $Z_o$ | The position parameters of origin $O'$ |
| $\alpha$, $\beta$ and $\lambda$ | The orientation parameters of origin $O'$ |
| $\boldsymbol{v_r} = [v_{r1}v_{r2}v_{r3}]^{\mathrm{T}}$ / $\boldsymbol{a}_r = [a_{r1}a_{r2}a_{r3}]^{\mathrm{T}}$ | The input velocity/acceleration |
| $\boldsymbol{J}/\boldsymbol{H}$ | The inverse velocity Jacobian/Hessian matrix |
| $\boldsymbol{J_\alpha}/\boldsymbol{H_\alpha}$ | The traditional Jacobian/Hessian matrix of limiteded-DOF PM |
| $\boldsymbol{J_v}/\boldsymbol{H_v}$ | The constraint Jacobian/Hessian matrix |
| $\boldsymbol{V}= [\boldsymbol{v}\ \boldsymbol{\omega}]^{\mathrm{T}}$/ $\boldsymbol{A}= [\boldsymbol{a}\ \boldsymbol{\varepsilon}]^{\mathrm{T}}$ | The output velocity/acceleration vector |
| $\boldsymbol{J}_{01}$ and $\boldsymbol{J}_{02}$ | The linear and angular velocity decoupling Jacobian matrices |
| $\boldsymbol{H}_1$ and $\boldsymbol{H}_2$ | The linear and angular acceleration decoupling Hessian matrix of $n$-DOF PM. |
| $F_{ai}$ | The active force |
| $F/T$ | Loading force/torque |
| $I_p$ | The polar moment of inertia |
| $F_{p1}$, $F_s$, $T_{ip}$ and $T_{iq}$ | The force/torque directly casing deformations |
| $\boldsymbol{\tau}_{ip}$ and $\boldsymbol{\tau}_{iq}$ | The unit vector of $\boldsymbol{T}_{ip}$ and $\boldsymbol{T}_{iq}$ |
| $s$ | A coefficient that represents the relationship between the constrained force/torque and its component |
| $\delta_{ri}$ | The longitudinal deformation along $r_i$ |
| $k_{ri}$ | A coefficient for mapping the relationships of $\delta_{ri}$ and $F_{ai}$ |
| $E$ | The modular of elasticity |
| $S_i$ | The area of $r_i$. |
| $\delta_{dpi}$ | The flexibility deformation in $r_i$ |
| $k_{pi}$ | A coefficient for mapping the relationships of $\delta_{dpi}$ and force |
| $I$ | The moment inertia |
| $\delta_{\theta ip}$ | The torsional deformation about $r_i$, |
| $k_{ip}$ | A coefficient for mapping the relationships of $\delta_{\theta ip}$ and torque |
| $G$ | The shear modulus |
| $k_{iq}$ | A coefficient for mapping the relationships of $\delta_{\theta iq}$ and torque |
| $\delta\boldsymbol{p} = [\delta x \delta y \delta z]^{\mathrm{T}}$, $\delta\Phi = [\delta\Phi_{\boldsymbol{x}}\delta\Phi_{\boldsymbol{y}}\delta\Phi_z]^{\mathrm{T}}$ | The linear and angular deformations of the moving platform |
| $\boldsymbol{W}$ | A coefficient matrix that represents the relationship between the constrained force/torque and the force/torque directly casing deformations |
| $\boldsymbol{K}^r$ | A coefficient matrix for mapping the relationships of deformation and force/torque |
| $\boldsymbol{K}_{6\times6}$ and $\boldsymbol{C}_{6\times6}$ | The stiffness matrix and compliance matrix |

## REFERENCES


[1] J. P. Merlet, *Parallel Robots*. London, U.K.: Kluwer, 2000, pp. 25–30.
[2] K. H. Hunt, "Structural kinematics of in-parallel-actuated robot-arms," *J. Mech., Transmiss., Autom. Des.*, vol. 105, no. 4, pp. 705–712, Dec. 1983.
[3] K. E. Neumann, "Robot," U.S. Patent 4 732 525, Mar. 22, 1986.
[4] K. E. Neumann, "Adaptive in-jig high load Exechon machining & assembly technology," SAE Tech. Papers 08AMT-0044, SAE International, 2008.
[5] T. Huang, M. Li, X. M. Zhao, J. P. Mei, D. G. Chetwynd, and S. J. Hu, "Conceptual design and dimensional synthesis for a 3-DOF module of the TriVariant—A novel 5-DOF reconfigurable hybrid robot," *IEEE Trans. Robot.*, vol. 21, no. 3, pp. 449–456, Jun. 2005.
[6] Y. G. Li, H. T. Liu, X. M. Zhao, T. Huang, and D. G. Chetwynd, "Design of a 3-DOF PKM module for large structural component machining," *Mechanism Mach. Theory*, vol. 45, no. 6, pp. 941–954, Jun. 2010.
[7] W. Liping, X. Huayang, G. Liwen, and Z. Yu, "A novel 3-PUU parallel mechanism and its kinematic issues," *Robot. Comput.-Integr. Manuf.*, vol. 42, pp. 102–106, Dec. 2016.
[8] L. Wang, H. Xu, and L. Guang, "Optimal design of a 3-PUU parallel mechanism with 2R1T DOFs," *Mech. Mach. Theory*, vol. 114, pp. 203–290, Aug. 2017.
[9] T. Sun and X. Huo, "Type synthesis of 1T2R parallel mechanisms with parasitic motions," *Mechanism Mach. Theory*, vol. 128, pp. 412–428, Oct. 2018.
[10] T. Huang, C. Dong, H. Liu, T. Sun, and D. G. Chetwynd, "A simple and visually orientated approach for type synthesis of overconstrained 1T2R parallel mechanisms," *Robotica*, vol. 37, no. 7, pp. 1161–1173, Jul. 2019.
[11] Y. Lu, N. Ye, and L. Ding, "Type synthesis of spatial 3-DoF parallel mechanisms with planar sub-chains using revised digital topological graphs and arrays," *Robotica*, vol. 35, no. 2, pp. 370–383, Feb. 2017.
[12] J. Gallardo-Alvarado and R. Rodriguez-Castro, "A new parallel manipulator with multiple operation modes," *J. Mech. Robot.*, vol. 10, no. 5, p. 51012, Oct. 2018.
[13] X. Jin, Y. Fang, D. Zhang, and X. Luo, "Design and analysis of a class of redundant collaborative manipulators with 2D large rotational angles," *Frontiers Mech. Eng.*, vol. 15, no. 1, pp. 66–80, Mar. 2020.
[14] X. Hu, F. Li, and G. Tang, "Kinematics analysis of 3UPU_UP coupling parallel platform in the marine environment," *IEEE Access*, vol. 8, pp. 158142–158151, 2020.
[15] G. Yang, R. Zhu, Z. Fang, C.-Y. Chen, and C. Zhang, "Kinematic design of a 2R1T robotic end-effector with flexure joints," *IEEE Access*, vol. 8, pp. 57204–57213, 2020.
[16] C. Gosselin, "Stiffness mapping for parallel manipulators," *IEEE Trans. Robot. Autom.*, vol. 6, no. 3, pp. 377–382, Jun. 1990.

[17] T. Huang, M. P. Mei, X. Y. Zhao, L. H. Zhou, D. W. Zhang, Z. P. Zeng, and D. J. Whitehouse, "Stiffness estimation of a tripod-based parallel kinematic machine," *IEEE Trans. Robot. Automat.*, vol. 18, no. 1, pp. 50–58, Feb. 2002.
[18] X. J. Liu, Z. L. Jin, and F. Gao, "Optimum design of 3-DOF spherical parallel manipulators with respect to the conditioning and stiffness indices," *Mech. Mach. Theory*, vol. 35, no. 9, pp. 257–267, 2000.
[19] D. Zhang and C. M. Gosselin, "Kinetostatic modeling of parallel mechanisms with a passive constraining leg and revolute actuators," *Mech. Mach. Theory*, vol. 37, no. 6, pp. 617–699, 2002.
[20] D. Zhang, "On stiffness improvement of the tricept machine tool," *Robotica*, vol. 23, no. 3, pp. 377–386, May 2005.
[21] S. K. Han, Y. F. Fang, and C. F. Huai, "Stiffness analysis of four degrees parallel manipulator," *Chin. J. Mech. Eng.*, vol. 42, pp. 31–34 and 42, May 2006.
[22] J. P. Merlet, "Jacobian, manipulability, condition number, and accuracy of parallel robots," *J. Mech. Des.*, vol. 128, no. 1, pp. 206–299, 2006.
[23] M. Wojtyra, "Joint reaction forces in multibody systems with redundant constraints," *Multibody Syst. Dyn.*, vol. 14, no. 1, pp. 43–46, 2005.
[24] B. Lian, T. Sun, Y. Song, Y. Jin, and M. Price, "Stiffness analysis and experiment of a novel 5-DoF parallel kinematic machine considering gravitational effects," *Int. J. Mach. Tools Manuf.*, vol. 95, pp. 82–96, Aug. 2015.
[25] T. Sun, H. Wu, B. Lian, Y. Qi, P. Wang, and Y. Song, "Stiffness modeling, analysis and evaluation of a 5 degree of freedom hybrid manipulator for friction stir welding," *Proc. Inst. Mech. Eng., C, J. Mech. Eng. Sci.*, vol. 231, no. 23, pp. 4441–4456, Dec. 2017.
[26] B. Hu and Z. Huang, "Kinetostatic model of overconstrained lower mobility parallel manipulators," *Nonlinear Dyn.*, vol. 86, no. 1, pp. 309–322, Oct. 2016.
[27] W. Liu, Y. Xu, J. Yao, and Y. Zhao, "The weighted Moore–Penrose generalized inverse and the force analysis of overconstrained parallel mechanisms," *Multibody Syst. Dyn.*, vol. 39, no. 4, pp. 363–383, Apr. 2017.
[28] Q. Li, L. Xu, Q. Chen, and X. Chai, "Analytical elastostatic stiffness modeling of overconstrained parallel manipulators using geometric algebra and strain energy," *J. Mech. Robot.*, vol. 11, no. 3, p. 31007, Jun. 2019.
[29] W.-A. Cao and H. Ding, "A method for solving all joint reactions of 3R2T parallel mechanisms with complicated structures and multiple redundant constraints," *Mechanism Mach. Theory*, vol. 121, pp. 718–730, Mar. 2018.
[30] Y. Li and Q. Xu, "Stiffness analysis for a 3-PUU parallel kinematic machine," *Mech. Mach. Theory*, vol. 43, no. 2, pp. 186–200, 2008.
[31] G. Cheng, P. Xu, D. Yang, and H. Liu, "Stiffness analysis of a 3CPS parallel manipulator for mirror active adjusting platform in segmented telescope," *Robot. Comput.-Integr. Manuf.*, vol. 29, no. 5, pp. 302–311, Oct. 2013.
[32] X. Shan and G. Cheng, "Static analysis on a 2(3PUS+S) parallel manipulator with two moving platforms," *J. Mech. Sci. Technol.*, vol. 32, no. 8, pp. 3869–3876, Aug. 2018.
[33] Z. Huang, Q. Li, and H. Ding, *Theory of Parallel Mechanisms*. Dordrecht, The Netherlands: Springer, 2012.
[34] Y. Lu and B. Hu, "Unification and simplification of velocity/acceleration of limited-DOF parallel manipulators with linear active legs," *Mechanism Mach. Theory*, vol. 43, no. 9, pp. 1112–1128, Sep. 2008.
[35] Y. Lu, Y. Shi, and B. Hu, "Solving reachable workspace of some parallel manipulators by computer-aided design variation geometry," *Proc. Inst. Mech. Eng., C, J. Mech. Eng. Sci.*, vol. 222, no. 9, pp. 1773–1781, Sep. 2008.